Coherent instability electron-cloud measurements

J.W. Flanagan, K. Ohmi, E. Benedetto, H. Fukuma, Y. Funakoshi, S. Hiramatsu, T. Ieiri, H. Ikeda, H. Jin, K. Oide, M. Tobiyama, E. Perevedentsev, +Others...

CESR-TA Collab. Mtg.

ILCDR08

Overview

- Summary of Single-bunch head-tail sideband signal measurements at KEKB
- Possibility of doing similar measurements at CesrTA

Single-bunch measurements: synchro-betatron sidebands

- Vertical betatron sidebands found at KEKB which appear to be signatures of fast head-tail instability due to electron clouds.
  - J.W. Flanagan, K. Ohmi, H. Fukuma, S. Hiramatsu, M. Tobiyama and E. Perevedentsev, PRL 94, 054801 (2005)
- Presence of sidebands also associated with loss of luminosity during collision.
  - J.W. Flanagan, K. Ohmi, H. Fukuma, S. Hiramatsu, H. Ikeda, M. Tobiyama, S. Uehara, S. Uno, and E. Perevedentsev, Proc. PAC05, p. 680 (2005)
- Further studies have also been performed:
  - Single beam studies:
    - Varying RF voltage
    - Varying chromaticity
    - Varying initial beam size below blow-up threshold (emittance)
    - Varying forced bunch excitation

Beam spectrum measurements

- Bunch Oscillation Recorder
  - Digitizer synched to RF clock, plus 20-MByte memory.
  - Can record 4096 turns x 5120 buckets worth of data.
  - Calculate Fourier power spectrum of each bunch separately.
- Inputs:
  - Feedback BPMs
    - 6 mm diameter button electrodes
    - 2 GHz ($4xf_{rf}$) detection frequency, 750 MHz bandpass
  - Fast PMT

Fourier power spectrum of BPM data

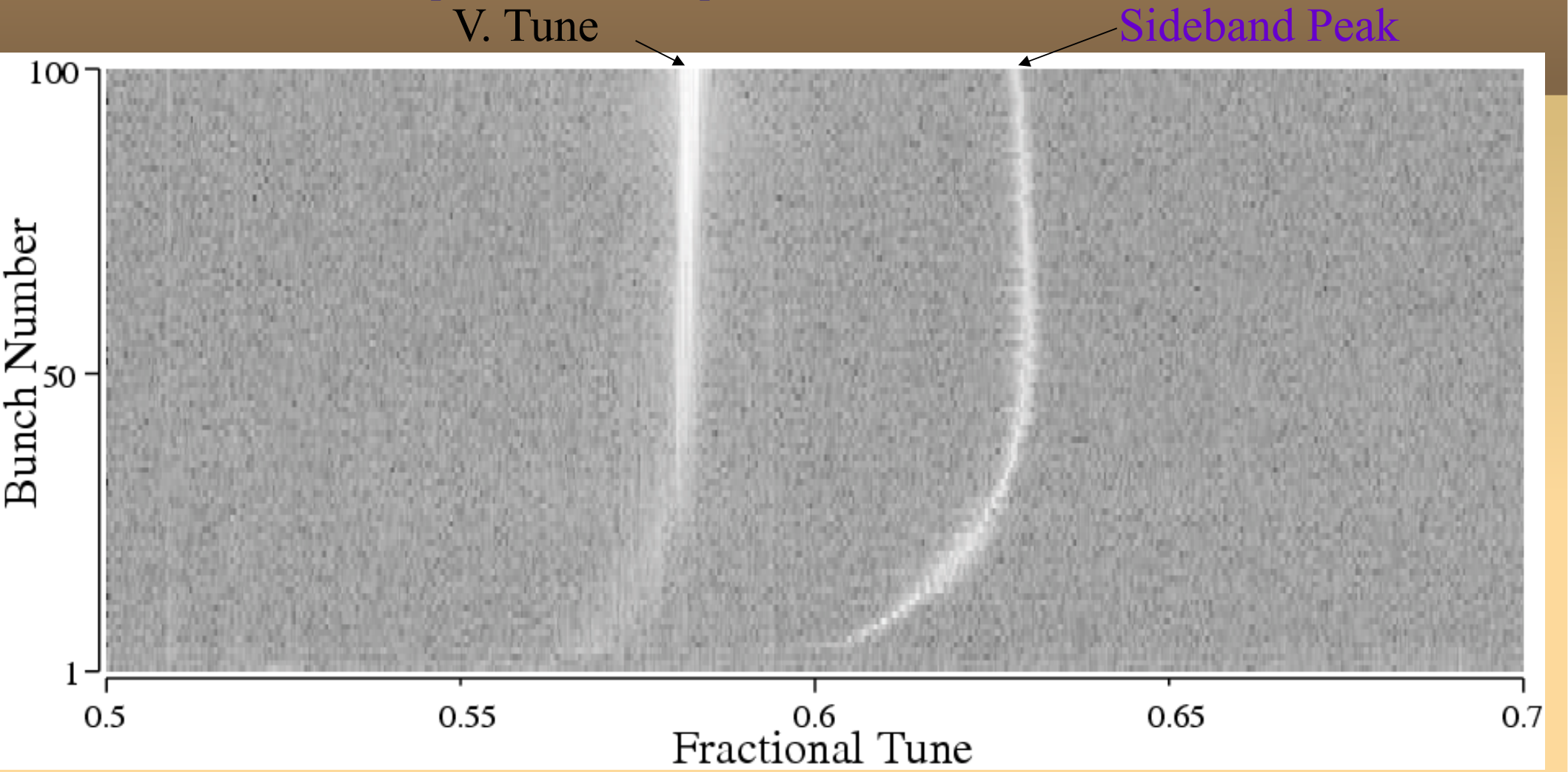

- LER single beam, 4 trains, 100 bunches per train, 4 rf bucket spacing
- Solenoids off: beam size increased from 60 μm ->283 μm at 400 mA
- Vertical feedback gain lowered
  - This brings out the vertical tune without external excitation

Bunch-by-bunch beam size along train as measured by gated camera

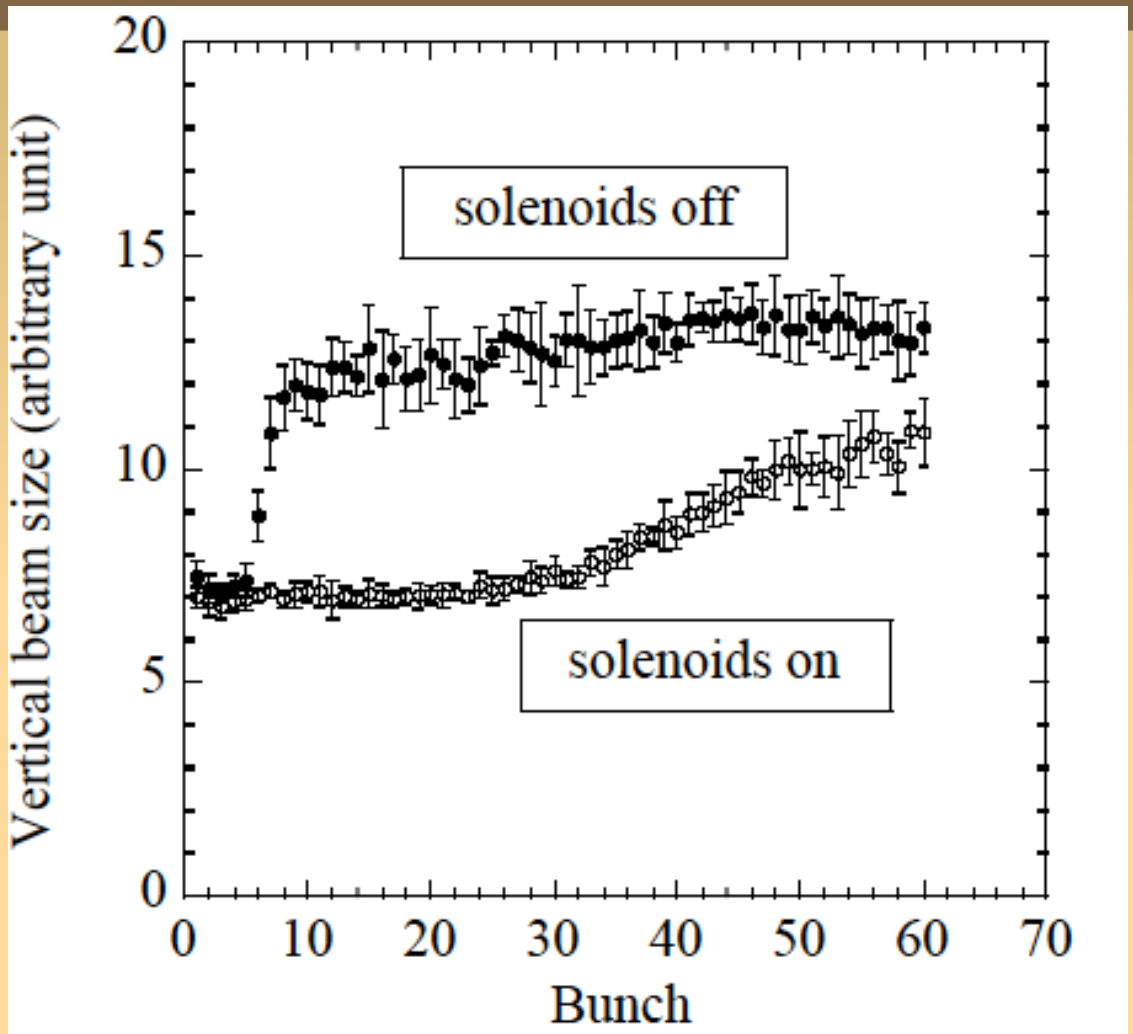

Figure 3: Vertical beam size along a train taken by the gated camera with and without solenoids. The train consisted of 60 bunches. Bunch spacing was 4 rf buckets. Bunch current was 0.67 mA.

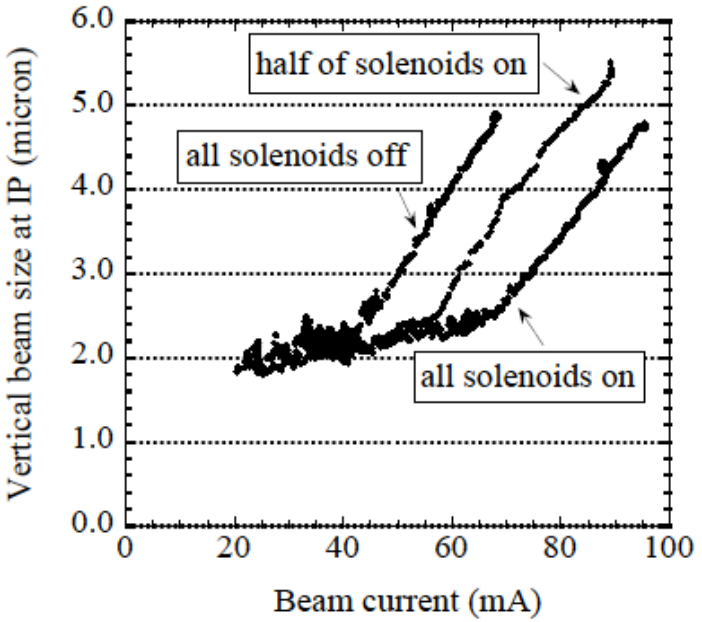

Figure 2: Vertical beam size as a function of the beam current. In the measurement two trains were injected on opposite sides in the ring. Each train contained 60 bunches. Bunch spacing was 4 rf buckets.

Fukuma et al., "Study of Vertical Beam Blow-up in KEKB LER," HEAC01 proceedings

←Model focusing wake

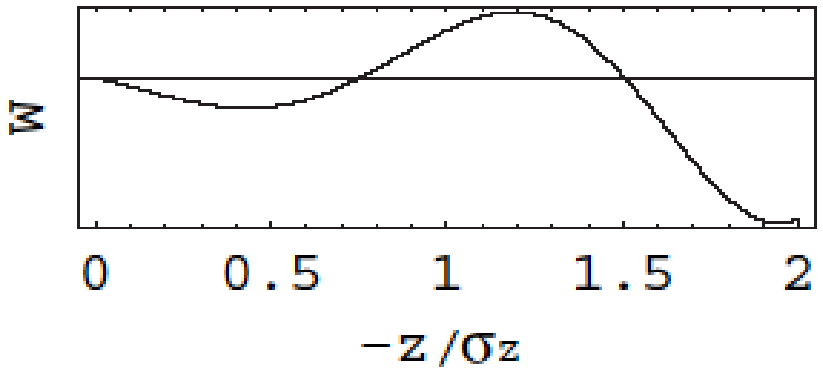

FIG. 5: Model focusing wake. The horizontal axis is longitudinal position normalized to the bunch length.

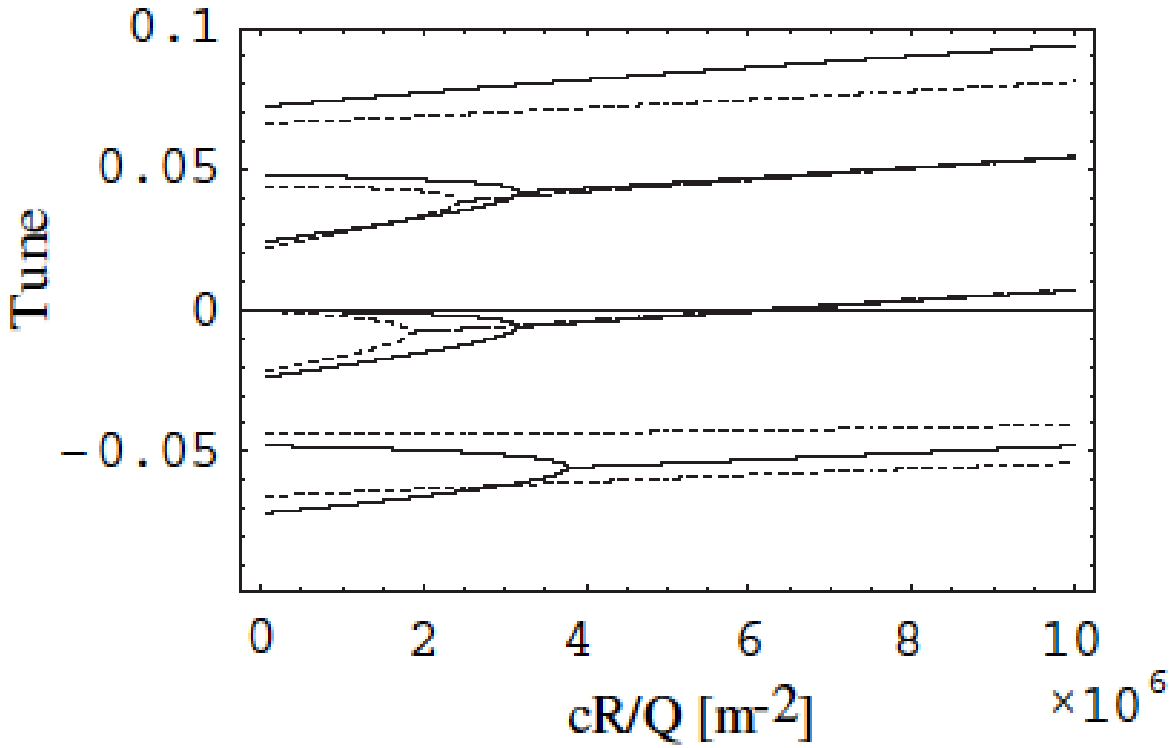

FIG. 6: Example mode spectrum for model focusing wake at $\nu_s = 0.022$ (dashed lines) and $\nu_s = 0.024$ (solid lines).

mode spectra were generated using a toy model with an airbag charge distribution and a simple effective wake, shown in Fig. 5, which uses a resonator-like wake W, increasing along $(-z)$ to represent the enhancement of the wake near the tail of the bunch due to pinching of the electron cloud:

$$W(z) = c\frac{R}{Q}e^{-\alpha z/c}\sin\omega_R\frac{z}{c}, \qquad (1)$$

wher $\alpha=w_R/2Q$, and $\omega_R = 2\pi \times 40$ GHz. (Note: the oscillation frequency of cloud electrons as calculated from the LER beam size and positron charge density is $\sim 2\pi \times 43$ GHz.)

←Mode spectrum using model wake and airbag charge distribution.

Sideband-betatron peak separation dependence on synchrotron tune reproduced.

Simulations of electron cloud induced head-tail instability

E. Benedetto, K. Ohmi

Simulation (PEHTS)

(HEADTAIL gives similar results)

Betatron sideband Tail of train

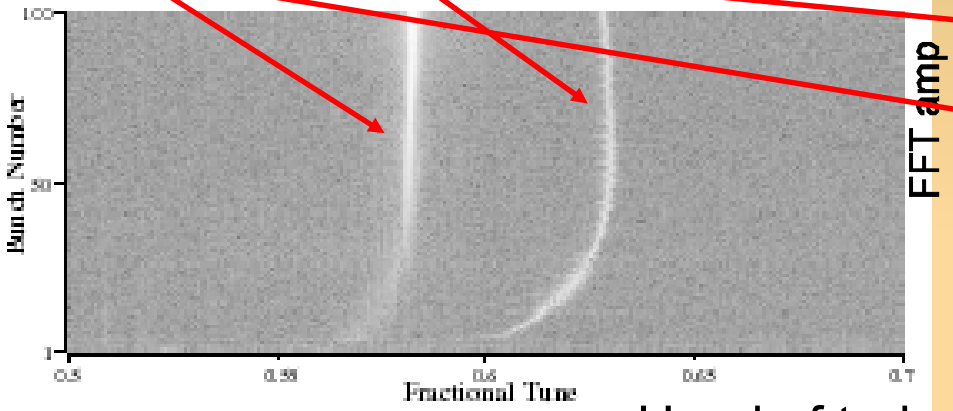

Head of train

FIG. 1. Two-dimensional plot of vertical bunch spectrum versus bunch number. The horizontal axis is the fractional tune, from 0.5 on the left edge to 0.7 on the right edge. The vertical axis is the bunch number in the train, from 1 on the bottom edge to 100 on the top edge. The bunches in the train are spaced 4-rf buckets (about 8 ns) apart. The bright, curved line on the left is the vertical betatron tune, made visible by reducing the bunch-by-bunch feedback gain by 6 dB from the level usually used for stable operation. The line on the right is the sideband.

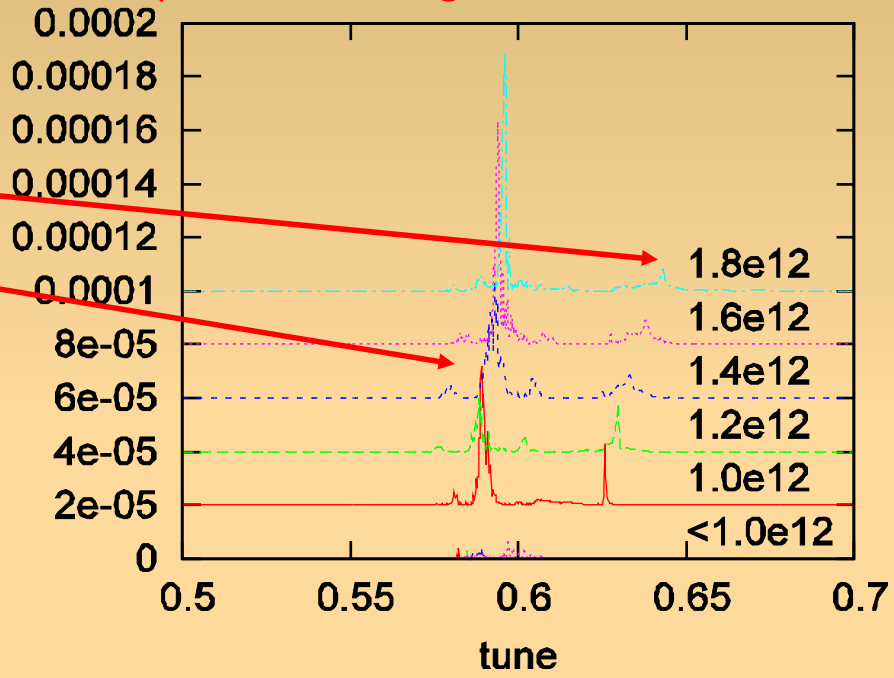

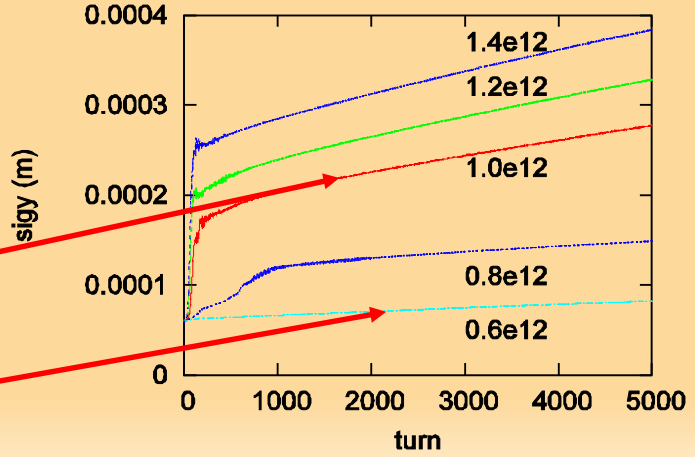

Head-tail regime

Incoherent regime

Feedback does not suppress sideband

- Bunch by bunch feedback suppresses only betatron amplitude.

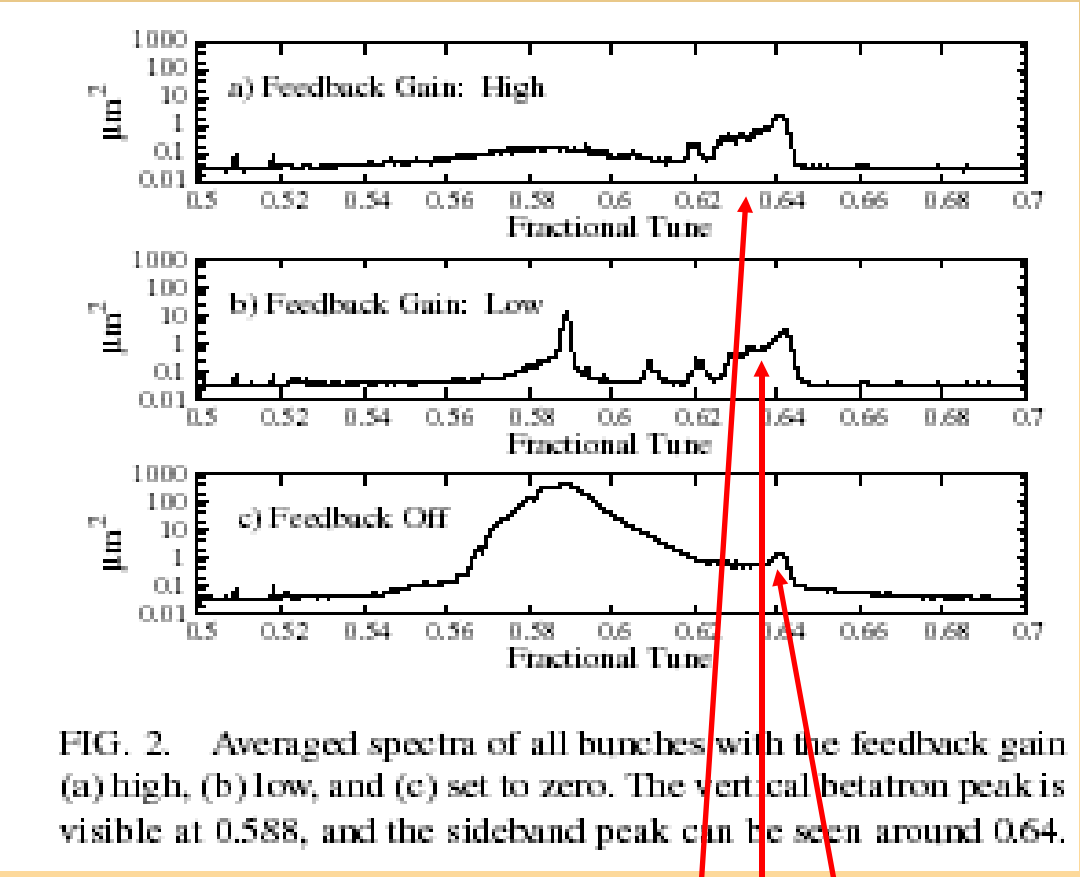

FIG. 2. Averaged spectra of all bunches with the feedback gain (a) high, (b) low, and (c) set to zero. The vertical betatron peak is visible at 0.588, and the sideband peak can be seen around 0.64.

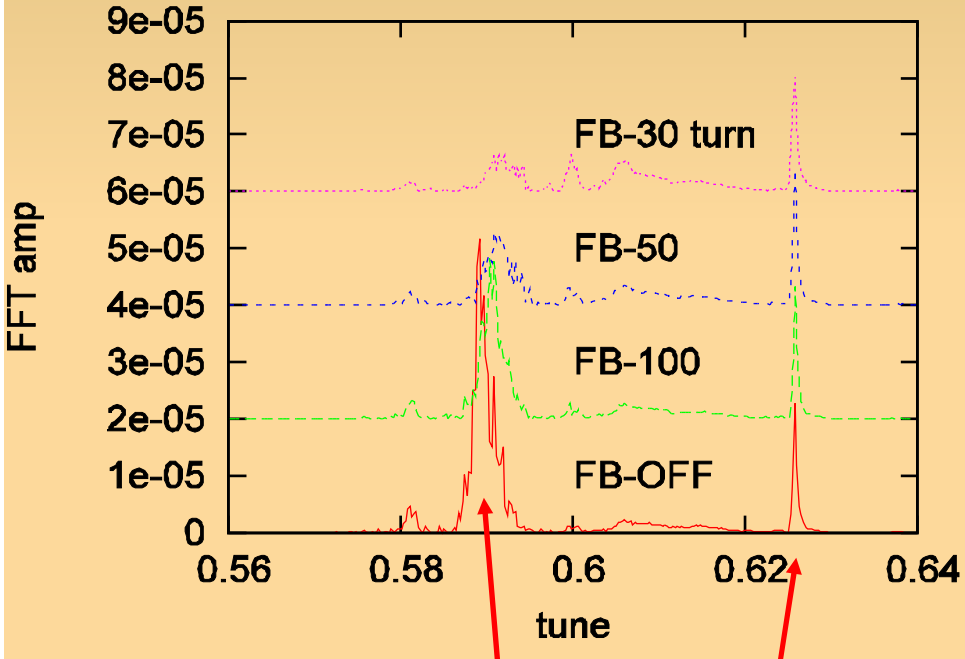

Simulation (PEHTS)

Sideband signal is Integrated over the train

PMT setup

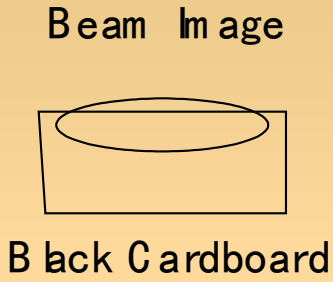

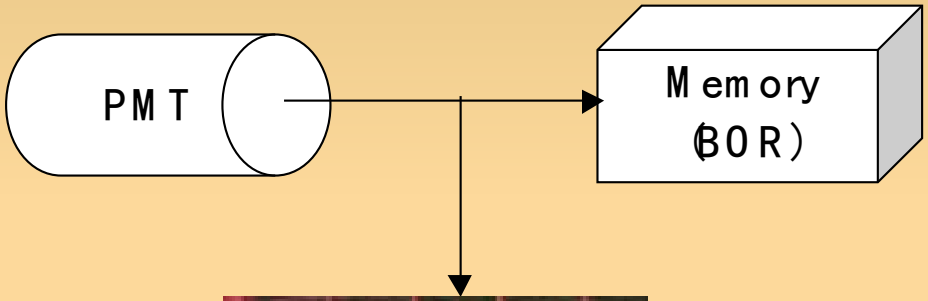

Partially block beam image with black cardboard, and measure light intensity of the visible part with a PMT. The PMT signal is buffered and then recorded using a feedback BOR digitizer/memory board.

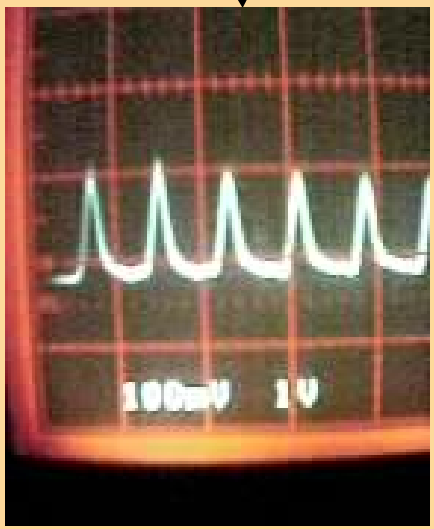

y: 100 mV/division
x: 10 ns/division

Beam Blow-up Measurement
4-bucket spacing, 600 bunches
4 trains, 150 bunches/train, 4 rf bucket spacing

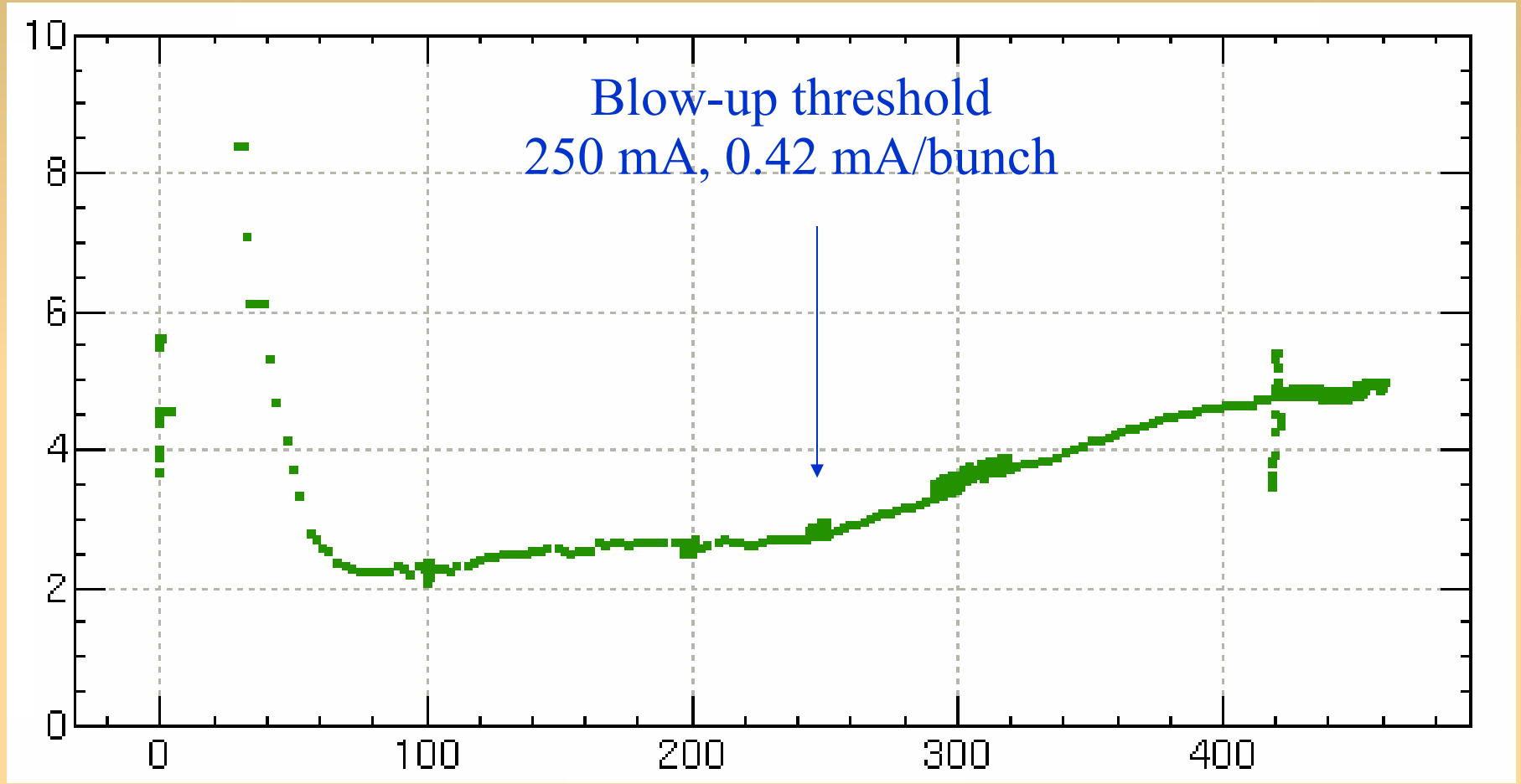

PMT Spectra

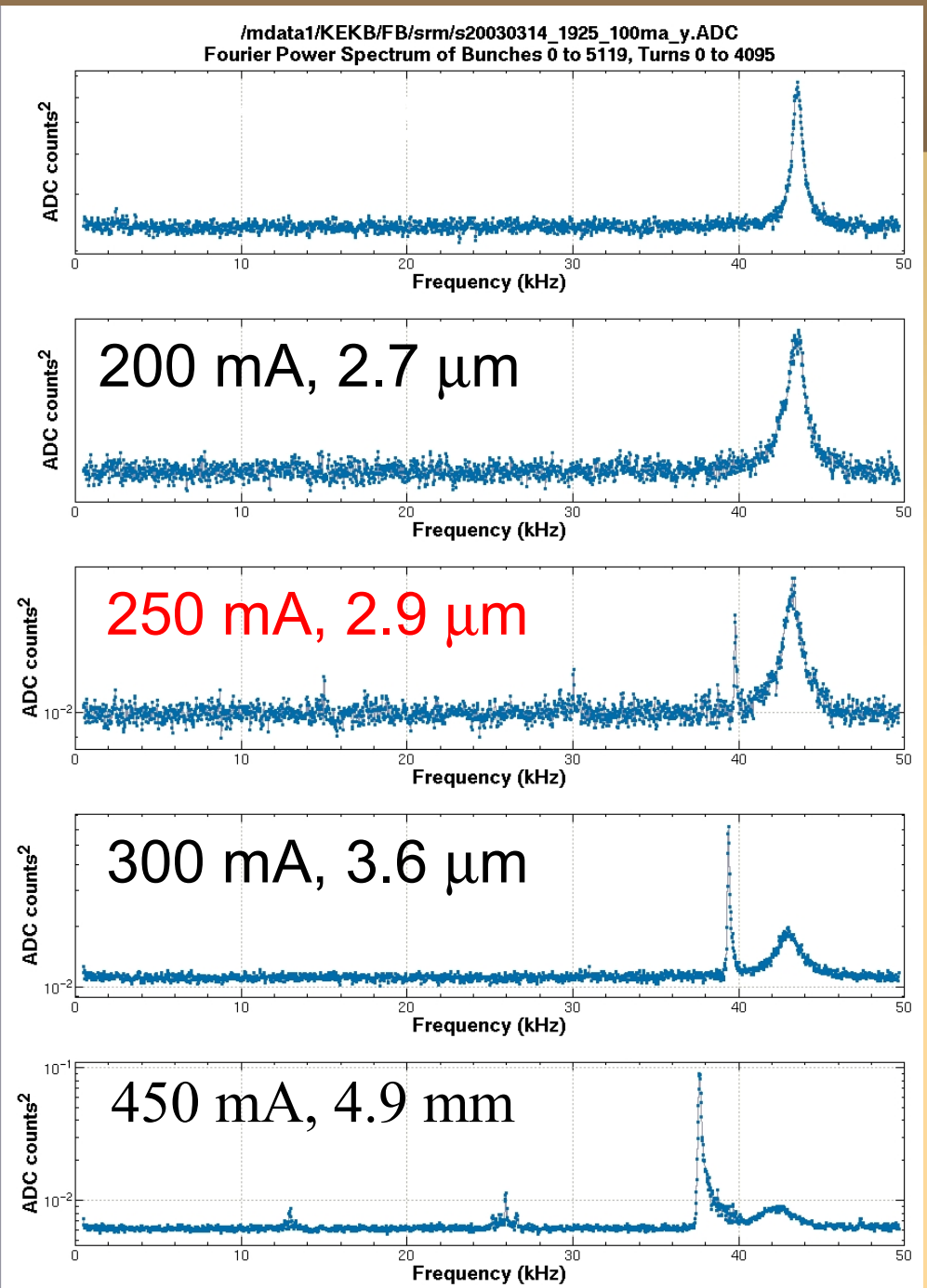

1.0 ←Tune 0.5

FB BPM Spectra

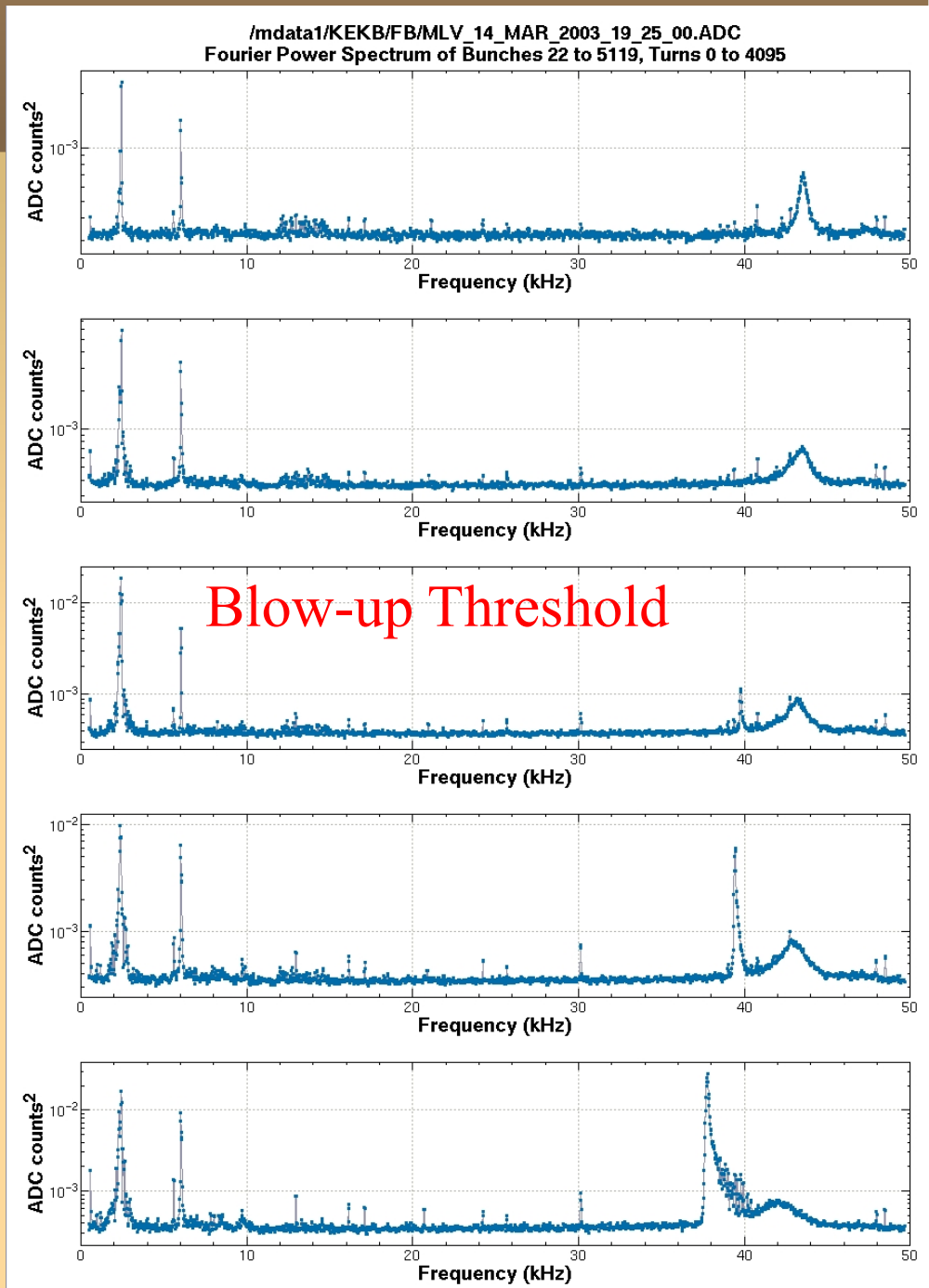

1.0 ←Tune 0.5

Time series data

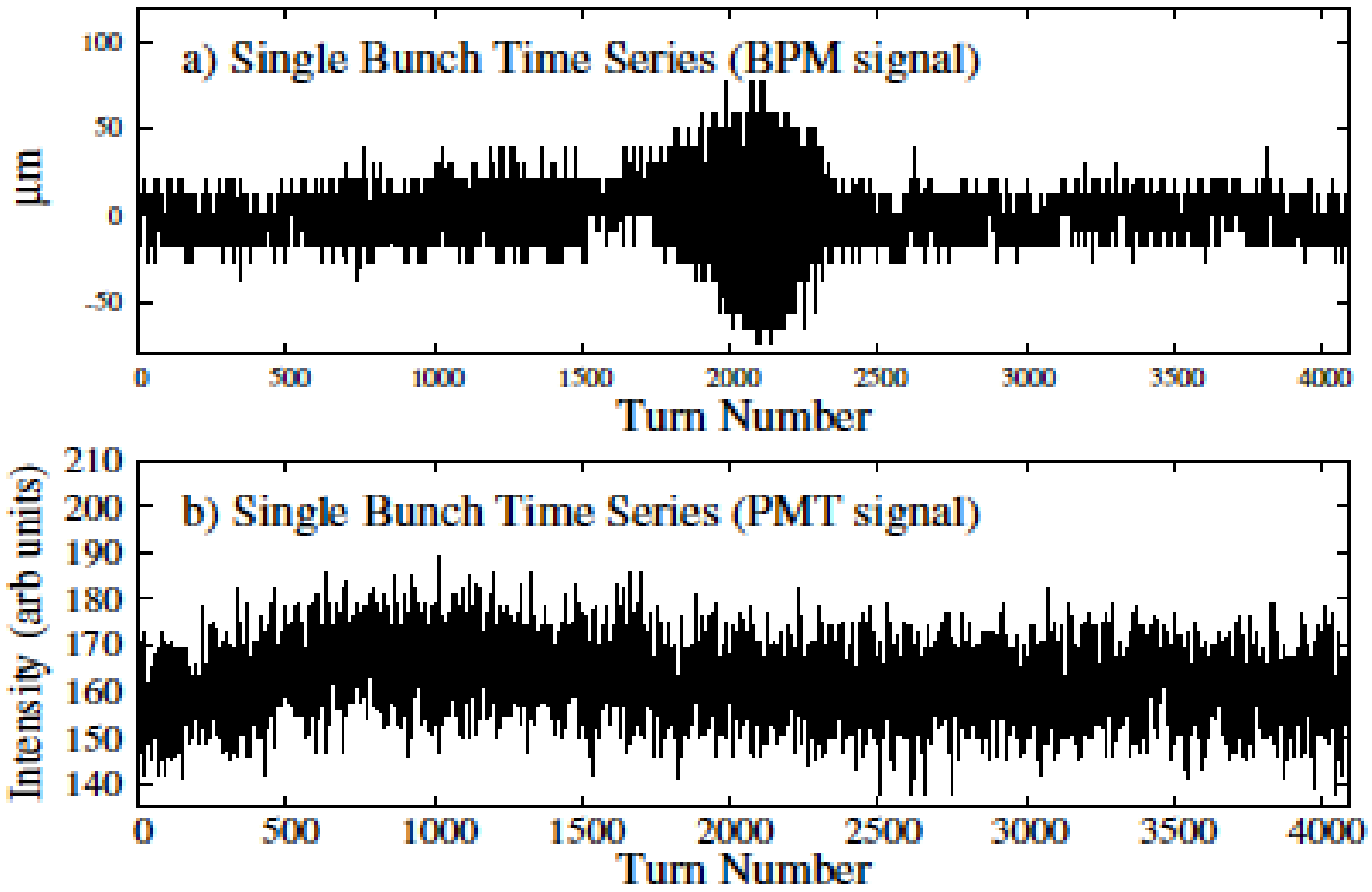

FIG. 4: Example time series of single bunches taken via a) BPM and b) PMT. Different bunches are shown for each detector; the data were taken within one minute of each other. A burst-like behavior is visible in the BPM signal. A fast ramp-up behavior with a similar rise-time as the BPM burst is seen in the PMT signal, followed by a gradual ramp-down.

BPM Data (Position)

PMT Data (Size)

Blow-up Pattern Analysis: PMT data

Find a bunch with characteristic blow-up pattern, and take spectra of 3 stages separately. Then average the 3 spectra over all bunches that have this pattern.

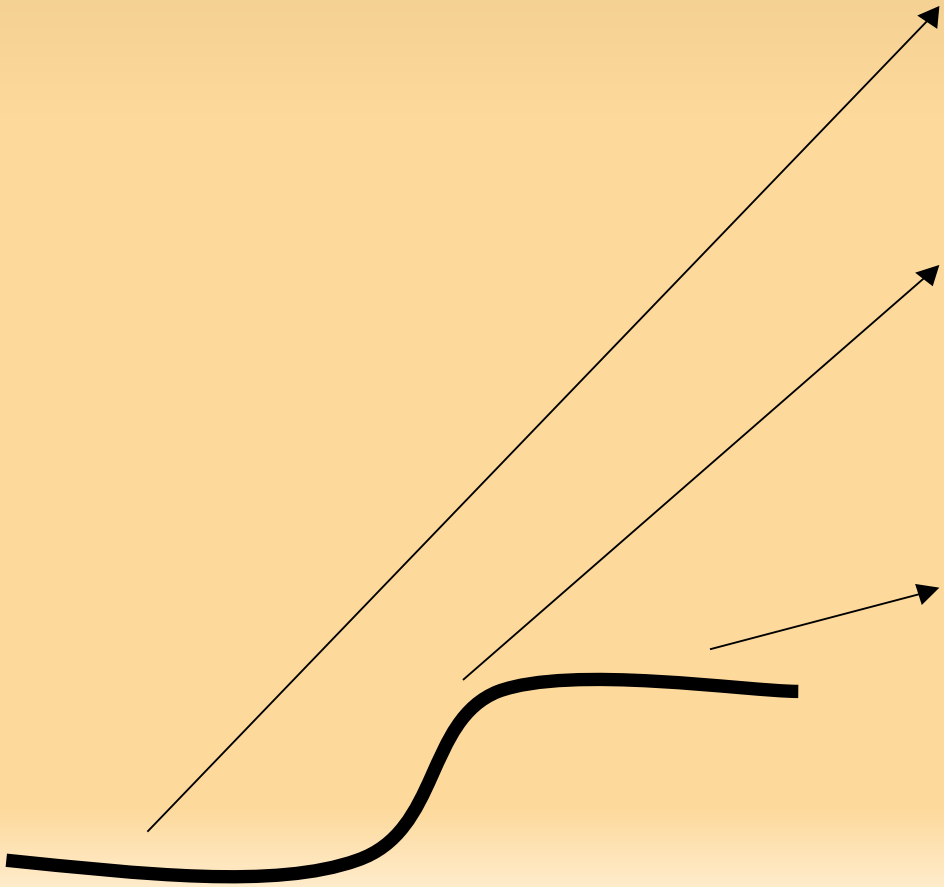

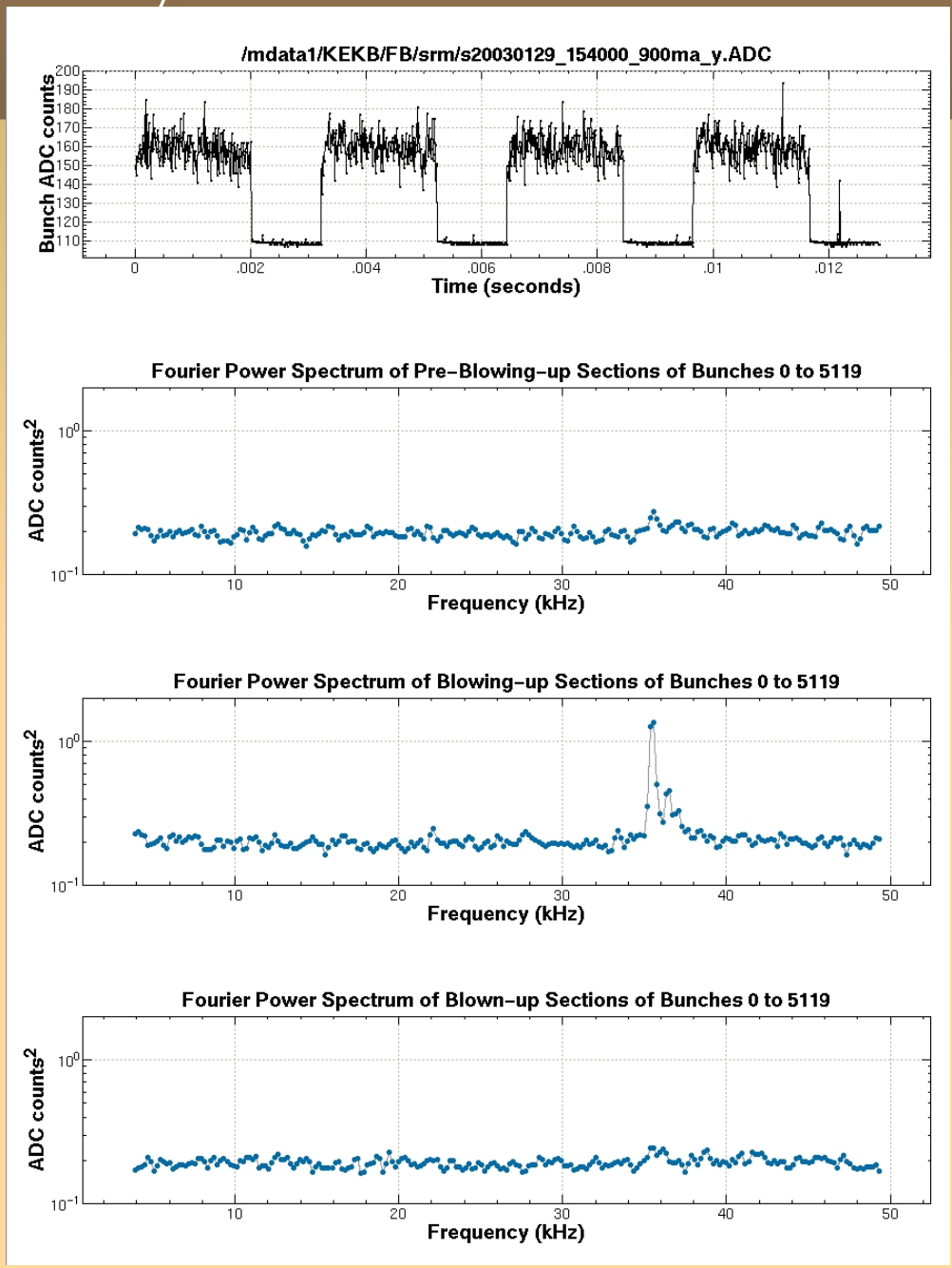

Summary of BPM + PMT measurements

- Sideband peak appears in **both** BPM and PMT measurements.
  - Two different types of detector
- Sideband peak appears in both instruments only at and above the beam-size blow-up threshold of beam current
  - Other measurements show that the amplitude of the sideband peak at constant beam current is affected by the strength of the solenoid field. Stronger solenoid field → smaller sideband peak.
- Sideband oscillation has a burst-like structure.
  - Sideband peak is present at a low level, then grows and damps in a burst lasting ~500 turns (5 ms).
  - During this burst, beam size grows ~5% from its already blown-up state
  - Immediately after burst is complete, sideband peak is absent, until beam size damps back down.

Effect of changing RF voltage

Separation is found to be close to $\Delta\nu_s$ towards the head of the train, and it decreases going towards the back of the train, where the cloud density is higher.

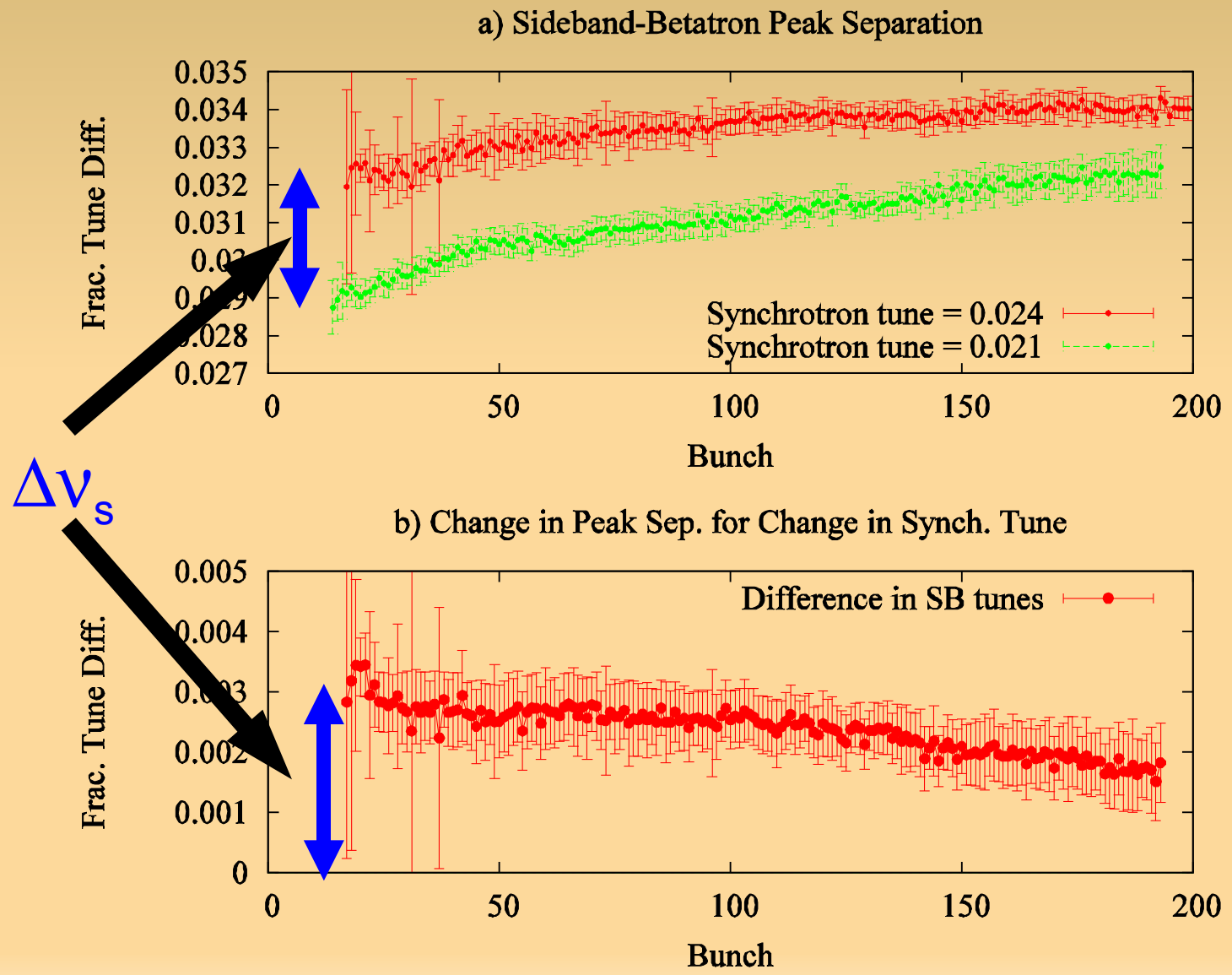

Sideband Peak Height Near Threshold at Diff. ν_s

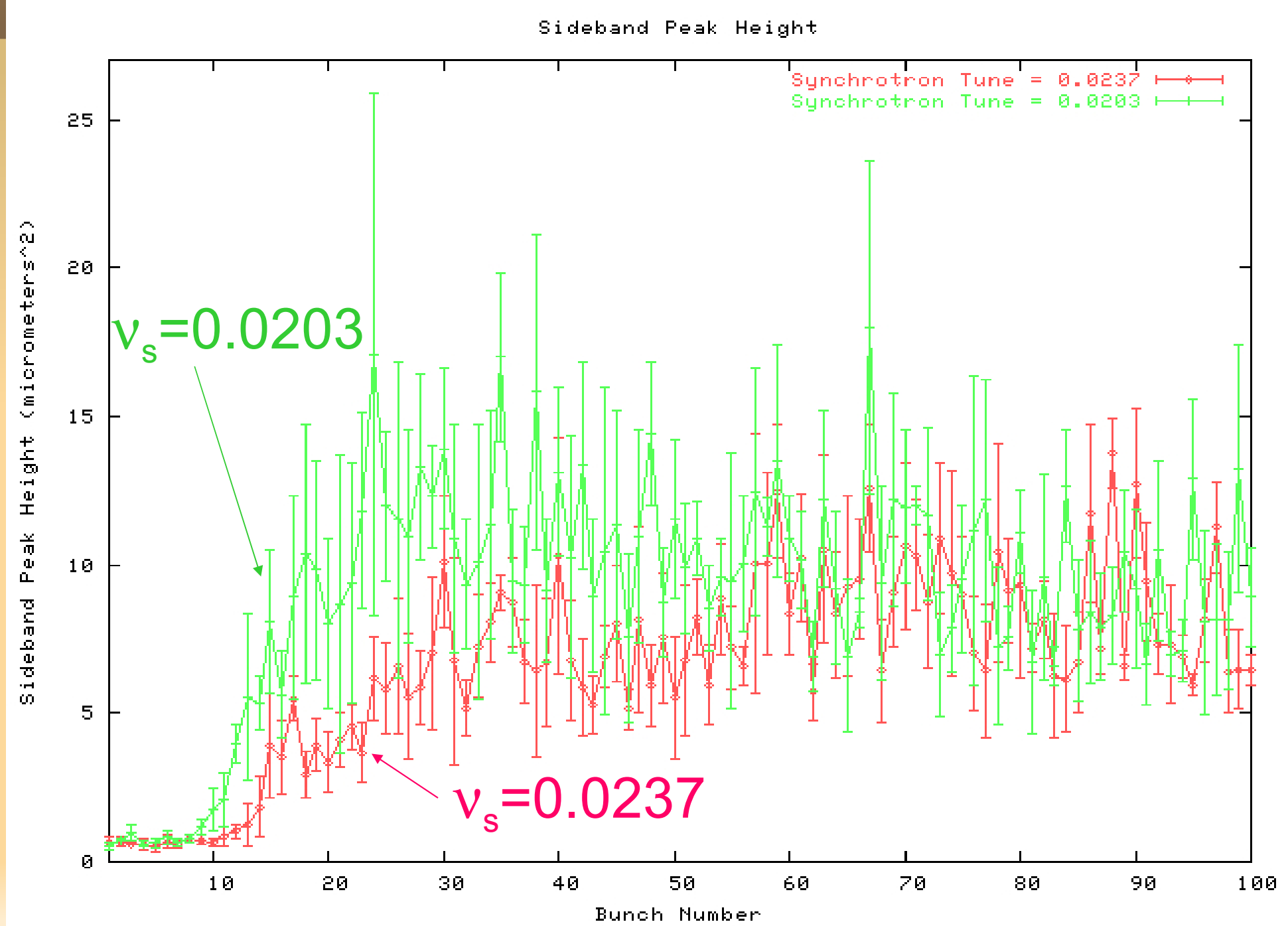

Model Spectrum

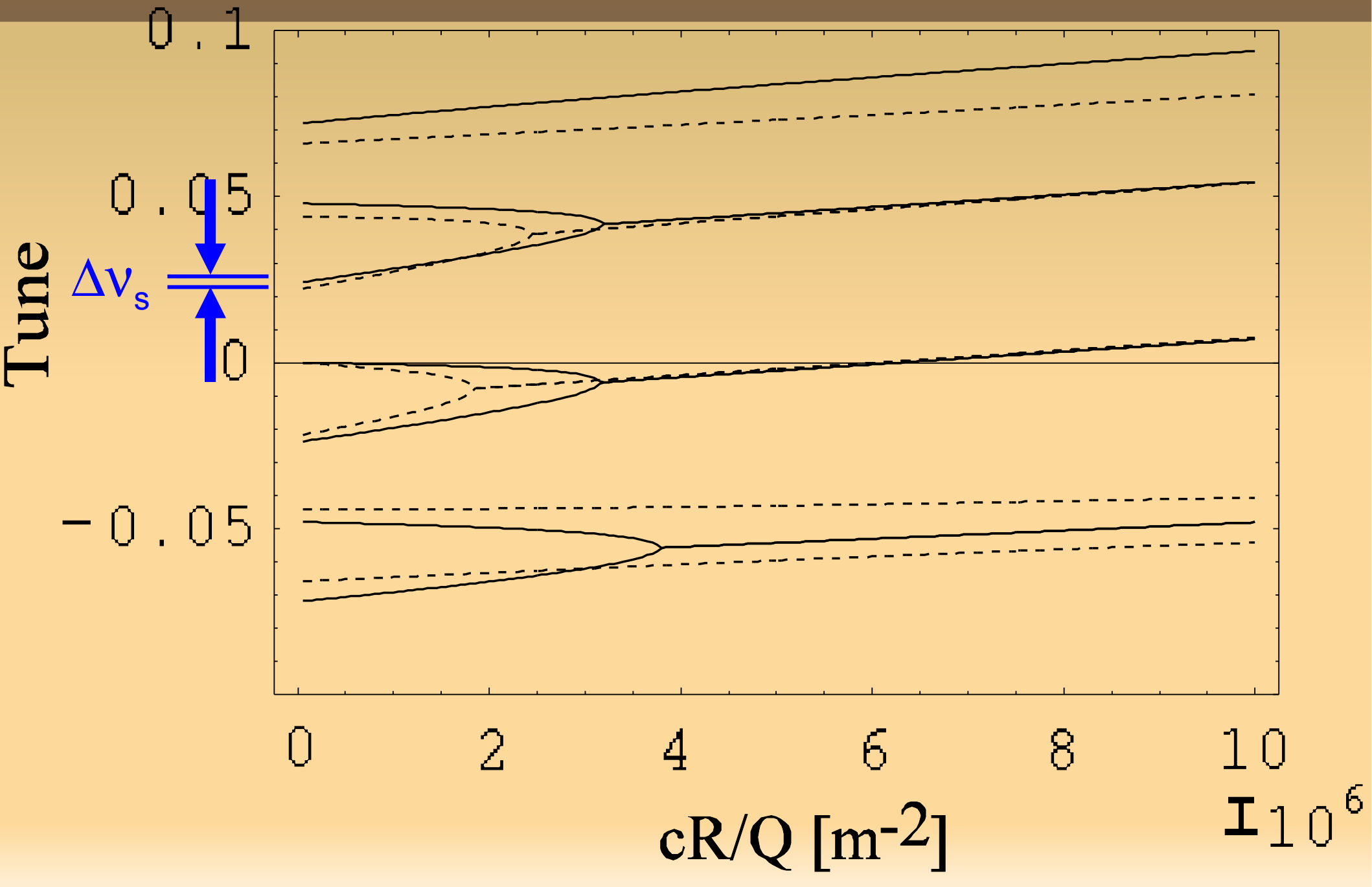

Effect of Changing ν_s (RF Voltage)

- Conclusion:
  - Threshold and separation between betatron peak and sideband peak are found to depend on ν_s, in agreement with model.

Sideband Peak Heights at Different Chromaticities

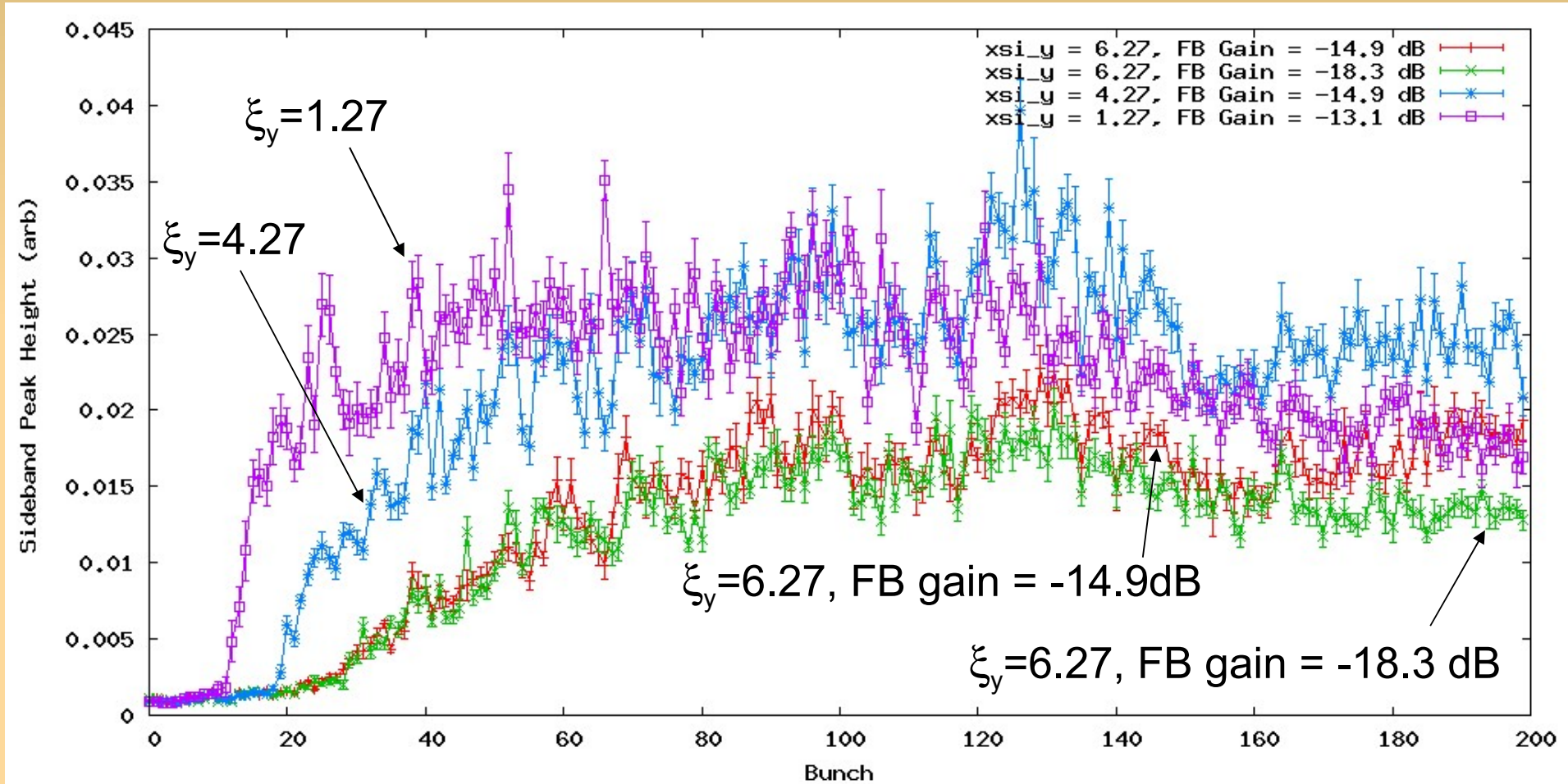

Effect of Changing Chromaticity

- **The lower the chromaticity, the earlier in the train the sideband appears.** (No change is seen for two different feedback gains at ξ_y=6.3, as expected.) Raising ξ_y from 1.3 to 4.3 pushes the onset of the instability back ~10 bunches along the train, as does further increasing ξ_y from 4.3 to 6.3. From simulations of electron cloud build-up (L.F. Wang, *et al*., PRSTAB **5** 124402 (2002)), these would correspond do changes in the electron cloud density of ~20-40%.
- In numerical simulations (K. Ohmi, Proc. 2001 PAC, Chicago, p. 1895 (2001)), changing ξ_y from 0 to 12 raises the threshold by a factor of 2, from 5×10^{11} electrons/m^3 to 1×10^{12} electrons/m^3. Scaling from this, each change in ξ_y used in the machine study would be expected to change the threshold by ~20.
  - **Basic agreement between simulations and experimental results.**

Effect of Changing Emittance

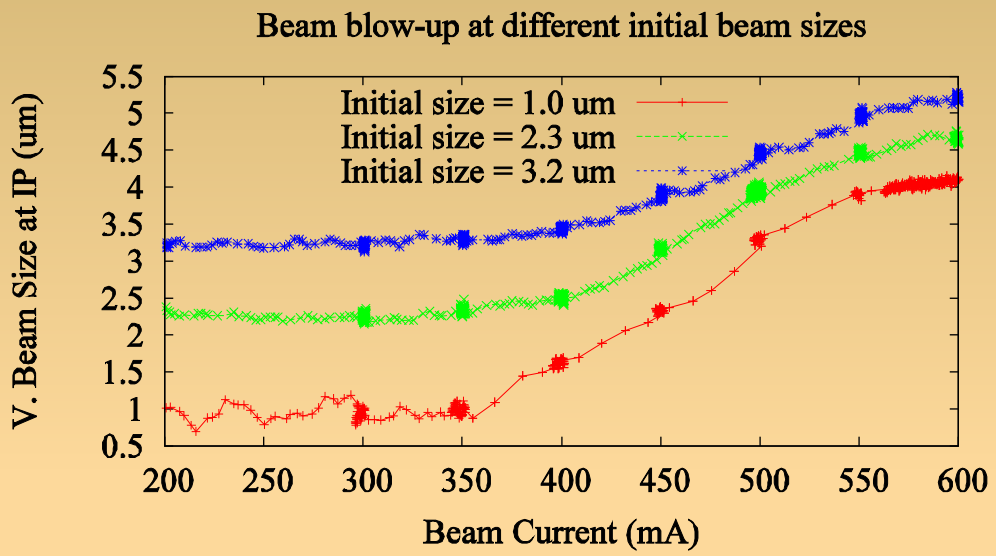

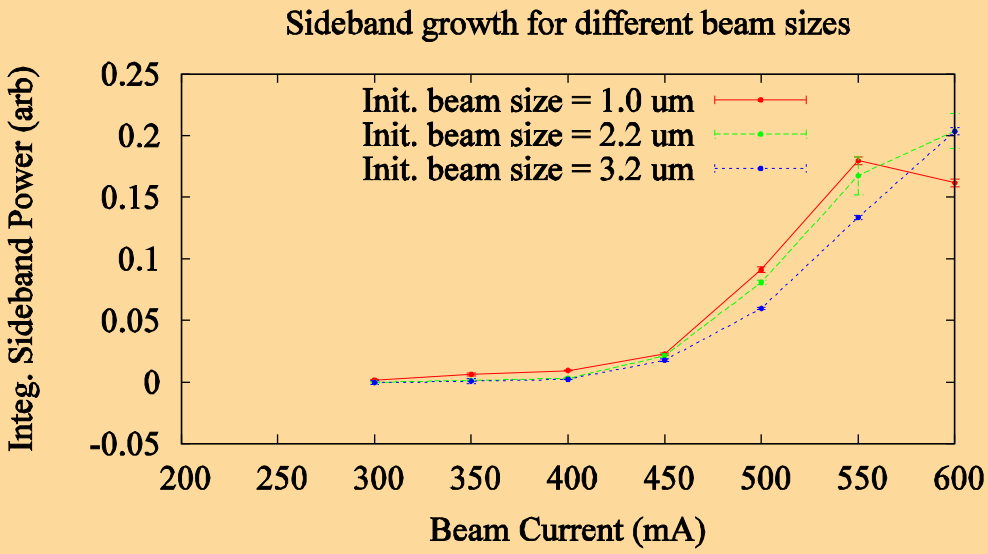

At a low current (200 mA) below the blow-up threshold, the vertical emittance of the beam was adjusted via dispersion bumps that are used for luminosity tuning. The beam size was set to 1, 2.3, and 3.2 μm (as expressed at the interaction point) in successive runs, and at each initial beam size the beam current was then ramped up to 600 mA while recording beam sizes and spectra.

➔**The instability threshold does not depend on initial beam size.**

Measurements at CesrTA

- Why:
  - Evaluation of the e-cloud induced head-tail instability threshold is critical in designing future machines.
  - At present, an unambiguous e-cloud induced head-tail instability signal has only been seen at one machine.
  - It is important to make sure that the scaling is understood.
- How can we measure the threshold at CesrTA?

Threshold of the strong head-tail instability (Balance of growth and Landau damping)

- Stability condition for $\omega_e\sigma_z/c>1$

$$\omega_e = \sqrt{\frac{\lambda_p r_e c^2}{\sigma_y(\sigma_x+\sigma_y)}}$$

$$U = \frac{\sqrt{3}\lambda_p r_0 \beta}{\nu_s \ \gamma \ \omega_e\sigma_z/c}\frac{|Z_\perp(\omega_e)|}{Z_0} = \frac{\sqrt{3}\lambda_p r_0 \beta}{\nu_s \ \gamma \ \omega_e\sigma_z/c}\frac{KQ}{4\pi}\frac{\lambda_e}{\lambda_p}\frac{L}{\sigma_y(\sigma_x+\sigma_y)} = 1$$

- Since $\rho_e=\lambda_e/2\pi\sigma_x\sigma_y$,

$$\rho_{e,th} = \frac{2\gamma\nu_s \ \omega_e\sigma_z/c}{\sqrt{3}KQr_0\beta L}$$

Origin of Landau damping is momentum compaction

- $Q=\min(Q_{nl}, \omega_e\sigma_z/c)$
  Q_{nl}=5-10?, depending on the nonlinear interaction.
- K characterizes cloud size effect and pinching.
- $\omega_e\sigma_z/c$~12-15 for damping rings.
- We use $K=\omega_e\sigma_z/c$ and $Q_{nl}=7$ for analytical estimation.

K. Ohmi

Parameters for Coherent Instability at CesrTA (Using cloud density = 1.5e11 m^-3 @ CESR-C

Parameter	Units	Cesr-C	CesrTA	CesrTA	CesrTA	CesrTA	CesrTA	How to create instability:	
Bunch current	mA	0.75	0.75	4.1	10	7	7	larger	
Bunch spacing	ns	14	14	4	9	14	14	smaller	
Energy	GeV	1.9	2	2	2	2	2	Insensitive	
σ_x	m	1.00E-03	1.50E-04	1.50E-04	1.50E-04	1.50E-04	1.50E-04	Insensitive	
σ_y	m	5.00E-05	1.00E-05	1.00E-05	1.00E-05	1.00E-05	1.00E-05	Insensitive	
σ_z	m	1.73E-02	9.00E-03	9.00E-03	9.00E-03	9.00E-03	9.00E-03	Insensitive	
ν_s		0.0487	0.098	0.098	0.098	0.049	0.098	smaller	RF voltage sensitive
β_y	m	30.00	10	10	10	10	20	larger	
Circumference L	m	768.44	768.44	768.44	768.44	768.44	768.44		
Current density	mA/ns	0.05	0.05	1.03	1.11	0.5	0.5		
γ		3718	3914	3914	3914	3914	3914		
Positrons/bunch N_p		1.20E+10	1.20E+10	6.56E+10	1.60E+11	1.12E+11	1.12E+11	Limit: ~2e11?	
λ_p		3.47E+11	6.67E+11	3.65E+12	8.89E+12	6.23E+12	6.23E+12		
ω_e		4.10E+10	3.25E+11	7.61E+11	1.19E+12	9.94E+11	9.94E+11		
Q_nl		7	7	7	7	7	7		
K=ω_e*σ_z/c		2.36	9.76	22.82	35.63	29.81	29.81		
Q=min(Q_nl,ω_e*σ_z/c)		2.36	7	7	7	7	7		
Threshold ρ_e,th	m^-3	1.36E+12	2.92E+12	2.92E+12	2.92E+12	1.46E+12	1.46E+12		
Cloud density	m^-3	1.48E+11	1.56E+11	2.98E+12	3.24E+12	1.46E+12	1.46E+12	< Assume scales w/curr. density, γ	

Instability achievable

Parameters for Coherent Instability at CesrTA (Using cloud density = 3.5e11 m^-3 @ CESR-C

Parameter	Units	Cesr-C	CesrTA	CesrTA	CesrTA	CesrTA	CesrTA	How to create instability:	
Bunch current	mA	0.75	0.75	1.7	6	3	3	larger	
Bunch spacing	ns	14	14	4	14	14	14	smaller	
Energy	GeV	1.9	2	2	2	2	2	Insensitive	
σ_x	m	1.00E-03	1.50E-04	1.50E-04	1.50E-04	1.50E-04	1.50E-04	Insensitive	
σ_y	m	5.00E-05	1.00E-05	1.00E-05	1.00E-05	1.00E-05	1.00E-05	Insensitive	
σ_z	m	1.73E-02	9.00E-03	9.00E-03	9.00E-03	9.00E-03	9.00E-03	Insensitive	
ν_s		0.0487	0.098	0.098	0.098	0.049	0.098	smaller	RF voltage sensitive
β_y	m	12.72	10	10	10	10	20	larger	
Circumference L	m	768.44	768.44	768.44	768.44	768.44	768.44		
Current density	mA/ns	0.05	0.05	0.43	0.43	0.21	0.21		
γ		3718	3914	3914	3914	3914	3914		
Positrons/bunch N_p		1.20E+10	1.20E+10	2.72E+10	9.61E+10	4.80E+10	4.80E+10	Limit: ~2e11?	
λ_p		3.47E+11	6.67E+11	1.51E+12	5.34E+12	2.67E+12	2.67E+12		
ω_e		4.10E+10	3.25E+11	4.90E+11	9.20E+11	6.51E+11	6.51E+11		
Q_nl		7	7	7	7	7	7		
K=ω_e*σ_z/c		2.36	9.76	14.69	27.6	19.52	19.52		
Q=min(Q_nl,ω_e*σ_z/c)		2.36	7	7	7	7	7		
Threshold ρ_e,th	m^-3	3.21E+12	2.92E+12	2.92E+12	2.92E+12	1.46E+12	1.46E+12		
Cloud density	m^-3	3.49E+11	3.68E+11	2.92E+12	2.94E+12	1.47E+12	1.47E+12	<-Assume scales w/curr. density, γ	

Instability achievable

Coherent Instability Threshold at CesrTA

- Parameters that are effective in lowering instability threshold/raising cloud density at CesrTA:
  - Bunch current: raise
  - Bunch spacing: lower
  - Synchrotron tune: lower
  - Beta y: raise
- Parameters that are ineffective:
  - Energy
  - Beam sizes (x,y,z)

Summary

- Vertical synchro-betatron sidebands found at KEKB LER, which are associated with electron-cloud induced beam blow-up.
- Signal has since been reproduced in simulation, supporting interpretation of it being a signature of head-tail instability.
- Further studies of threshold dependence on ξ_y and ν_s and sideband-betatron separation dependence on ν_s show basic agreement with simulations.
- Found no apparent threshold dependence on $\sigma_{y0.}$
- **Measurement of how coherent instability threshold scales is critical to design of future machines.**
  - **This should be possible at CesrTA**
  - **==>This should be done at CesrTA**

A first peek at coded aperture data

J.W. Flanagan, J.P. Alexander,
H. Fukuma, S. Hiramatsu, H. Ikeda, K. Kanazawa,
T. Mitsuhashi, J. Urakawa, G.S. Varner,
M.A. Palmer

CESR-TA Collab. Mtg.
ILCDR08

With thanks to:
Jim Savino, Aaron Lyndaker, Dan Peterson,
Mike Billing

Outline

1) Motivation
2) Coded Aperture Imaging Principles
3) Design Considerations: diffraction and transmission
4) Prototype, plans and VERY PRELIMINARY test results

Motivation

- In considering the possibility of doing low-emittance e-cloud studies for the ILC Damping Ring at the KEKB LER, a beam size measurement system with the following requirements was specified:
  - High (few um) resolution.
  - High-speed: bunch-by-bunch readout (2 ns) desired
    - => High flux throughput (wideband, large aperture)
  - Low dependence of magnification on beam current
- Optical systems at KEKB do not seem up to the task.
- As at CesrTA, we were led to consider an X-ray monitor.

X-Ray Monitor

- Used or under development at ATF, CESR-TA, Spring-8, PEP-II, elsewhere.
- A Fresnel zone plates is typically used as an X-ray lens
  - Requires the use of a monochromator
    - Sensitive to heat load
      - ==>Beam current dependence
    - Cuts available light level down drastically (1%), necessitating long exposure times
- To maximize bandwidth and minimize number of components, we are considering the use of **coded aperture imaging.**

Coded Aperture Imaging

- A coded aperture is a mask used to modulate incoming light.
- A pinhole is the simplest type of coded aperture, requiring no monochromator (good), but with very small aperture (bad).
- In 1968 R.H. Dicke (APJL, 153, L101, 1968) proposed the use of a random array of pinholes for X-ray and gamma-ray astronomy. The resulting image needs to be deconvolved back through the mask pattern to reconstruct the source distribution on the sky.
- Improved mask designs were then developed, most notably the Uniformly Redundant Array (URA) mask, which has the nice property that its auto-correlation is a delta function (no sidelobes), and it can achieve open aperture areas of up to 50%.
  - Good overview at: http://astrophysics.gsfc.nasa.gov/ca

Modified URA Mask, Anti-mask, and Cross-correlation

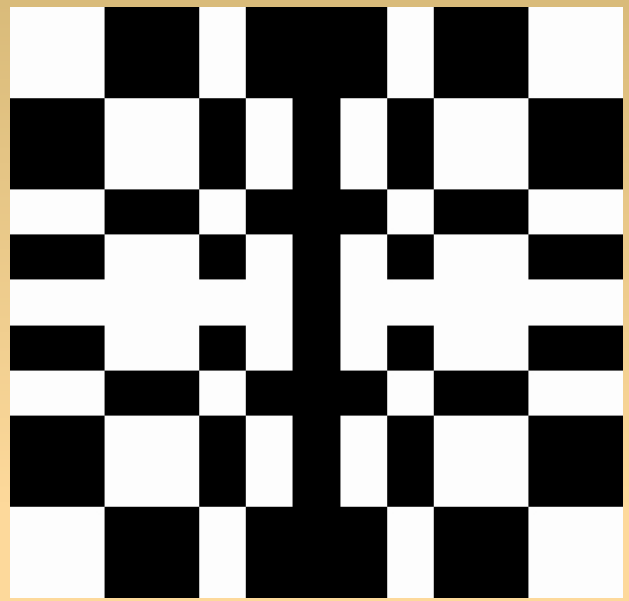

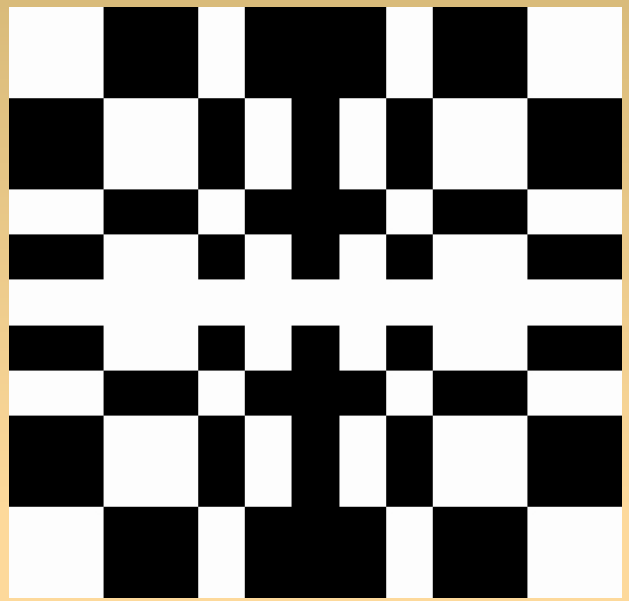

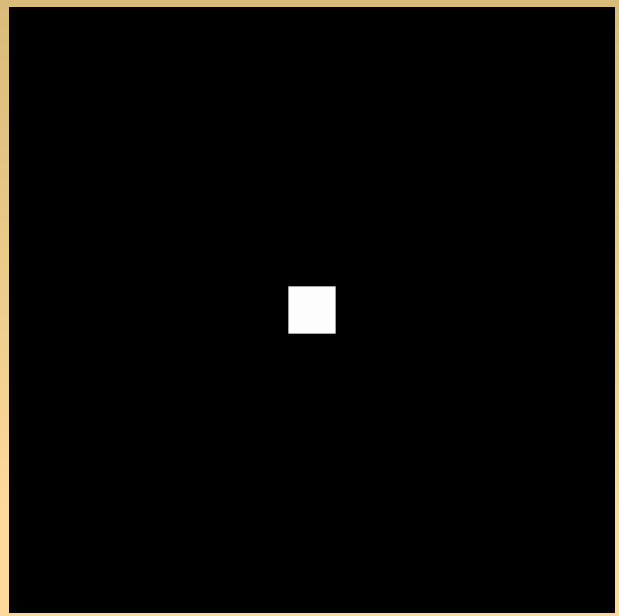

- Image is encoded using mask and decoded using anti-mask, where cross-correlation between mask and anti-mask is delta function.
- Pixel transparency determined by Jacobi function:
  - Is (pixel index)%DIM == (i*i)%DIM for any 1<i<DIM?
    - Yes/No->Open/Closed.
    - 2-D case based on inverse XOR of both indices.
- Note: Fresnel zone plates can in principle also be used as coded apertures. (Barrett, H.H., Horrigan, F.A.: 1973, Appl. Opt., 12, 2686)

Coded Aperture Decoding

In order to perform digital analysis of the picture, Eq. (4) must be quantized. Define $O(i,j)$ to be an array whose elements represent the number of photons observed during the exposure time in an area equal to that of a single pinhole from a $\Delta\alpha\Delta\beta$ region of the source centered at $(i\Delta\alpha, j\Delta\beta, b)$. Let $\Delta\alpha = \Delta\beta = c/f$ rad where each pinhole in the aperture is a c by c square hole. Define $A(i,j)$ to be an array with each element denoting the presence or absence of a pinhole in the aperture. If there is a hole at $(i \cdot c, j \cdot c)$, $A(i,j)$ has the value one, otherwise it is zero. The possible locations for the pinholes are restricted to a grid of discrete points with a spacing equal to c.

Equation (4) can be approximated to have the same form as Eq. (1):

$$P(k,l) \cong O * A + N \equiv \sum_i \sum_j O(i,j)A(i+k, j+l) + N(k,l), \quad (5)$$

where $P(k,l)$ should be interpreted as the number of photons received from the object in an $m \cdot c$ by $m \cdot c$ area of the detector centered at $(k \cdot m \cdot c, l \cdot m \cdot c)$ plus some noise $N(k,l)$.

The P array is measured experimentally and since the A array is known, Eq. (5) is used to determine an estimate of the object intensity distribution. In the correlation analysis methods, the reconstructed object is determined from P and A by

$$\hat{O}(i,j) = P * G \equiv \sum_k \sum_l P(k,l)G(k+i, l+j), \quad (6)$$

where G will be chosen such that $A * G$ is approximately (or exactly) a delta function.

The above is applicable to all coded aperture techniques. We will now employ the above in the implementation of URAs.

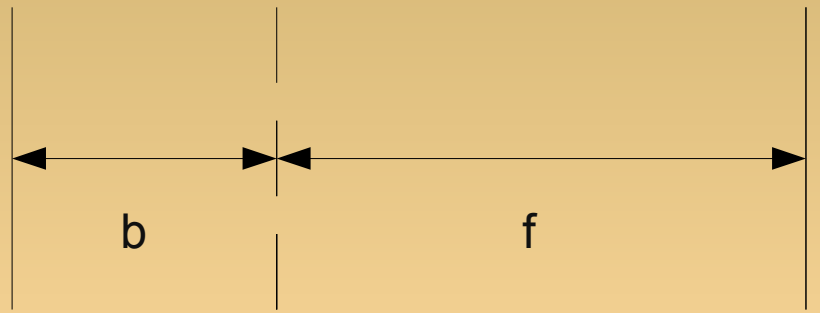

Source
pix. size
= c(b+f)/f

Mask
min. hole size
= c

Detector
pix. size
= c(b+f)/b

- Magnification m=(b+f)/b

- Fenimore and Cannon, Appl. Optics, V17, No. 3, p. 337 (1978)

Illustrative Example

Source Image Detector Image Reconstruction

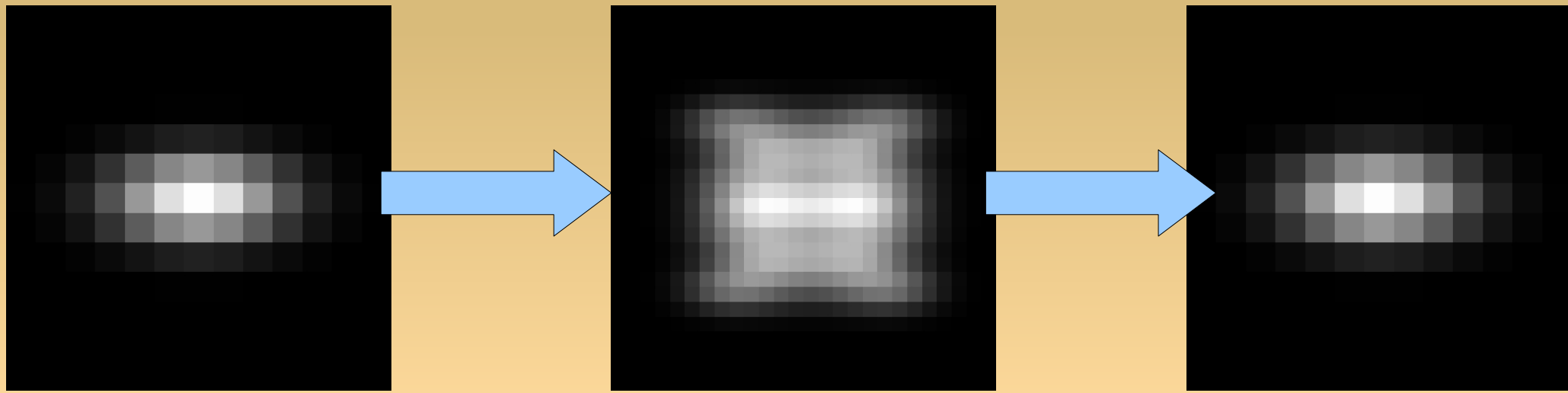

Reconstructed Horizontal and Vertical Profiles

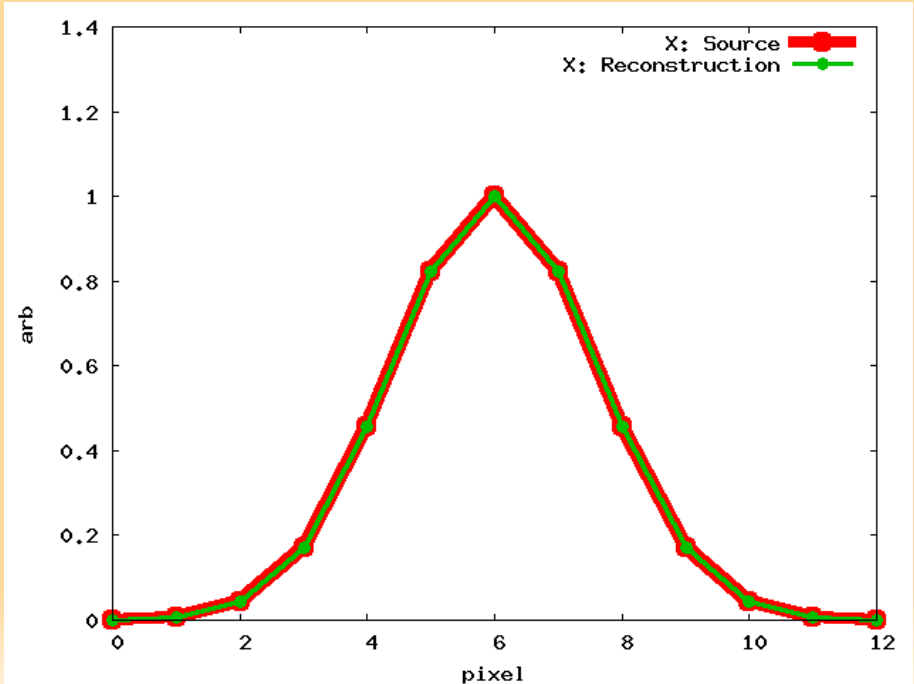

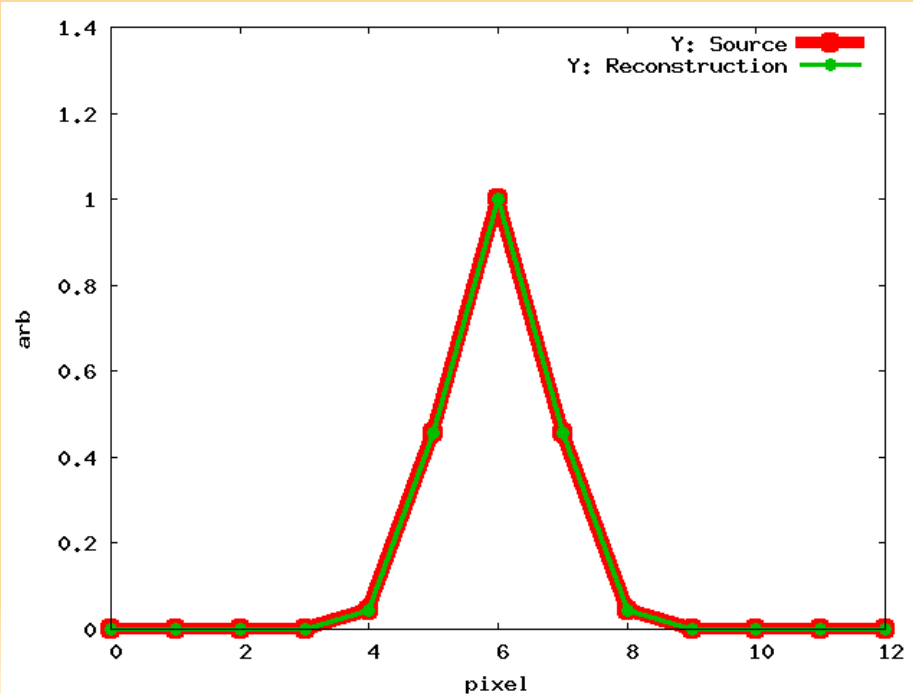

Coded Aperture Imaging (cont.)

- Several reconstruction methods are in use: inversion, cross-correlation, photon tagging (back-projection), Wiener filtering, and iterative methods such as the Maximum Entropy Method and Iterative Removal of Sources (IROS).
- Coded aperture imaging is now a well-established technique in X-ray astronomy, with scattered applications outside that field, e.g.:
  - Medical imaging, thermal neutron imaging, inertial confinement monitoring, and nuclear blast monitoring
- URA masks have been used for the measurement of phase coherence of undulator radiation (J.J.A. Lin et al., PRL 90, 074801), and of an x-ray laser (J. E. Trebes, et al., PRL 68, 588–591 (1992). The URA was essentially used as a multi-slit interferometer for monochromatic light (not wideband).
- **Our goal: to develop wideband coded aperture techniques which could be useful for general beam profile diagnostics at CesrTA, SuperKEKB, and elsewhere.**

Vertical-only mask: 1x31

Much faster reconstruction when using iterative methods (1-D vs 2-D problem)

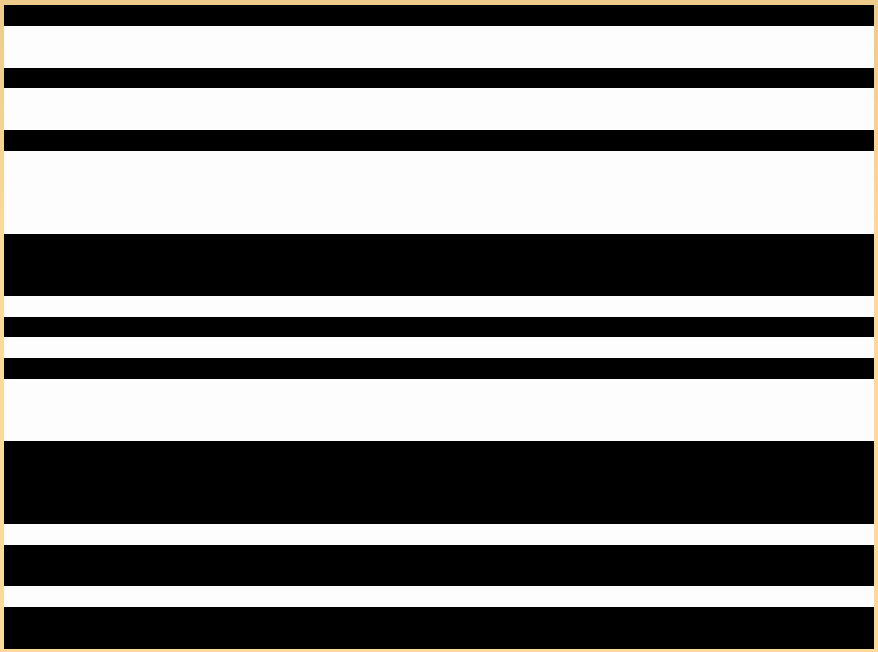

1-D URA Mask

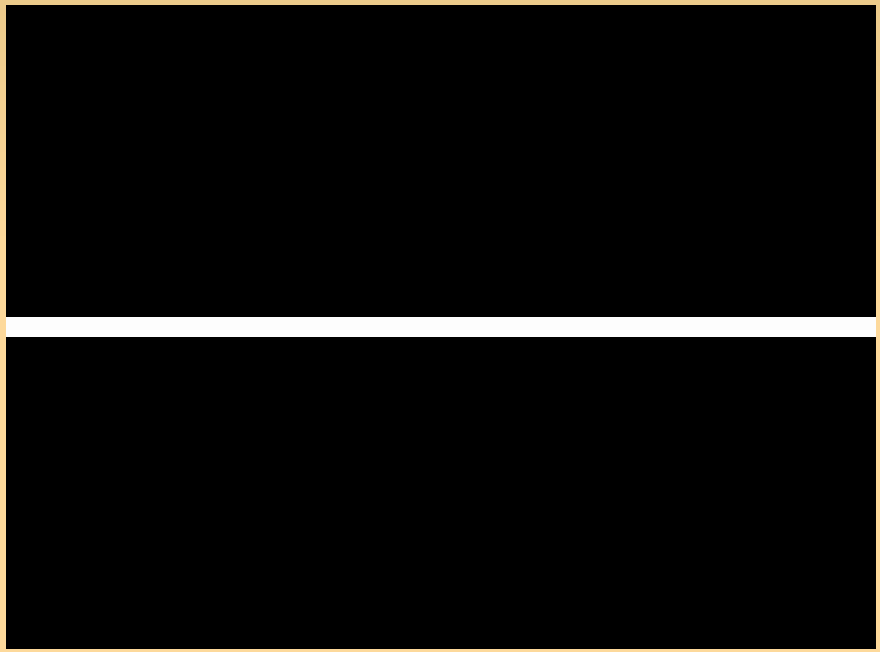

Autocorrelation

X-Ray Flux for KEKB in ILCDR study mode

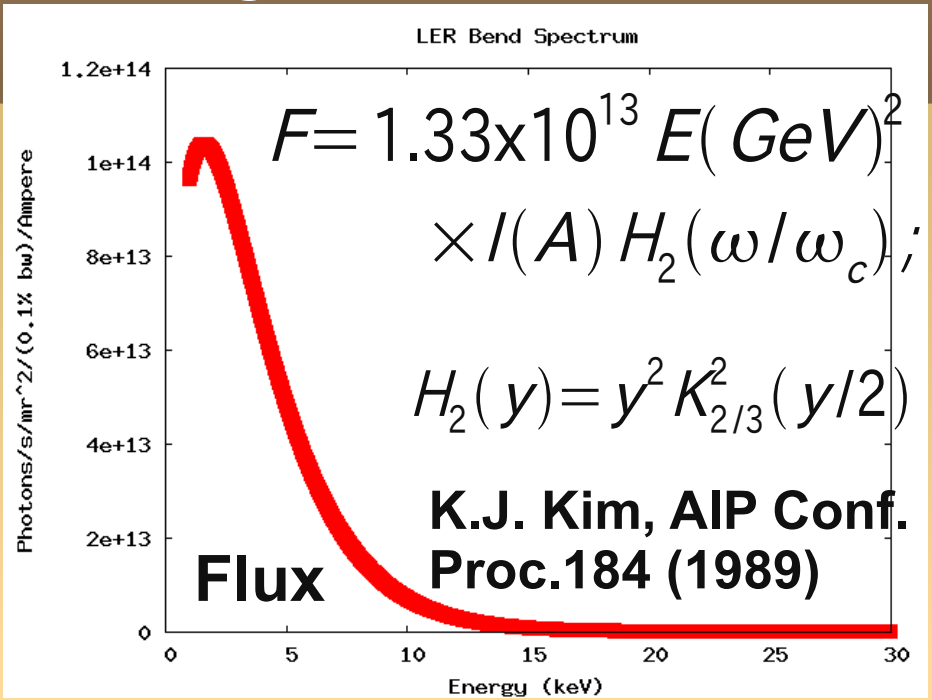

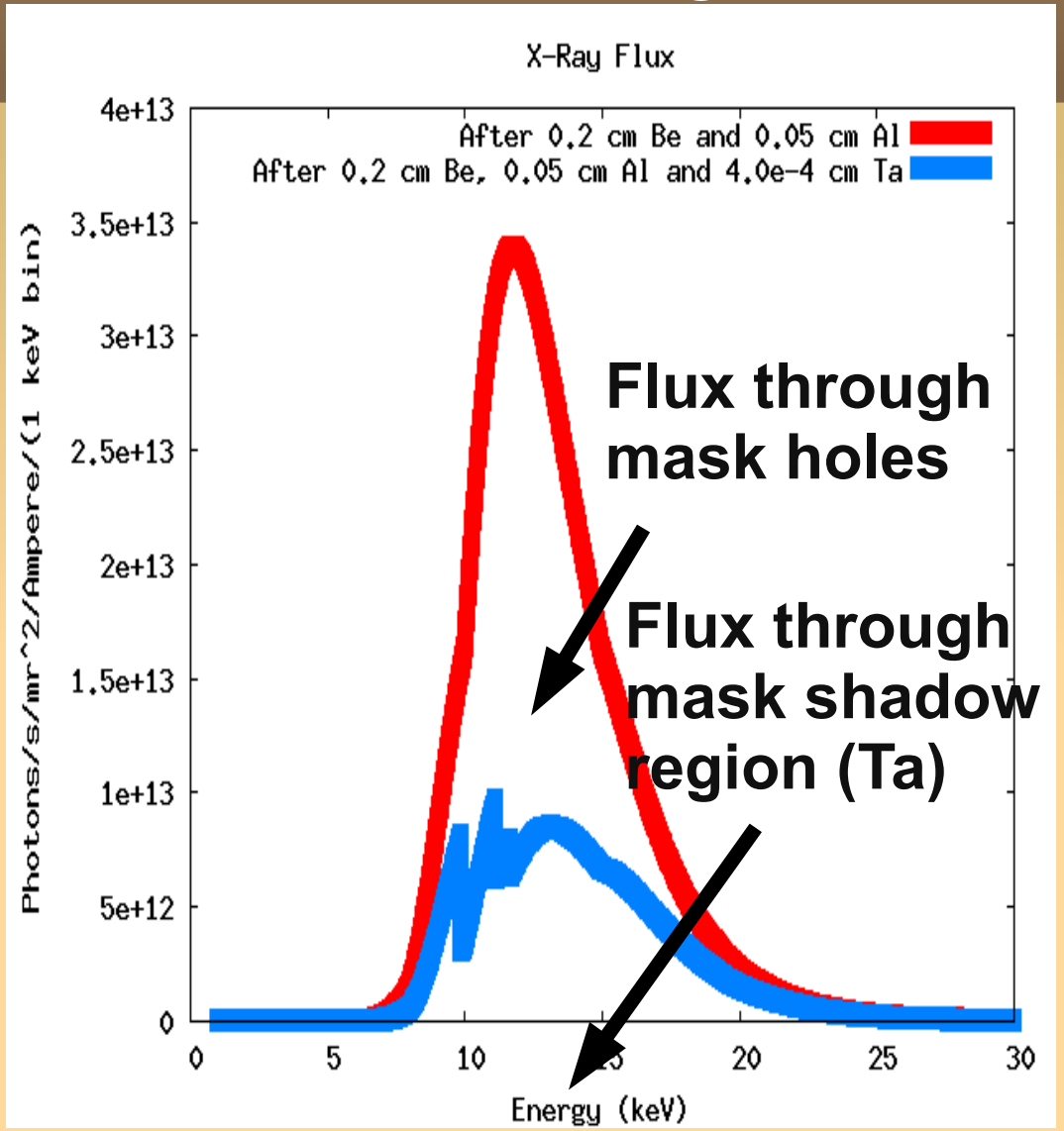

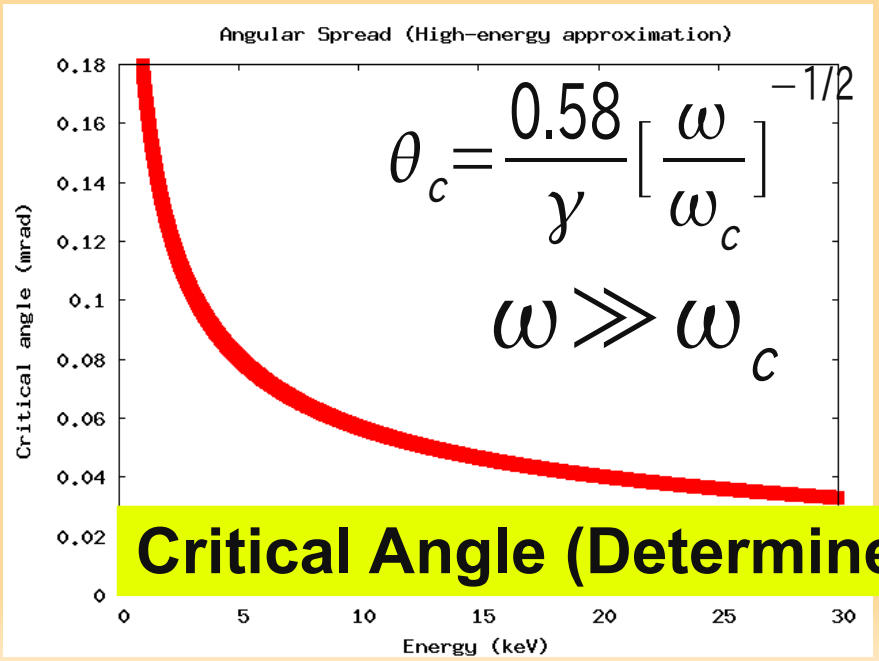

Signal 1626.2 photons/turn/mA
Background 566.748 photons/turn/mA

Critical Angle (Determines usable mask size)

Diffraction cannot be ignored
Vertical-only mask: 1x31, 4 um min. aperture

Irradiance as function of photon energy. Mask->detector = 24 m

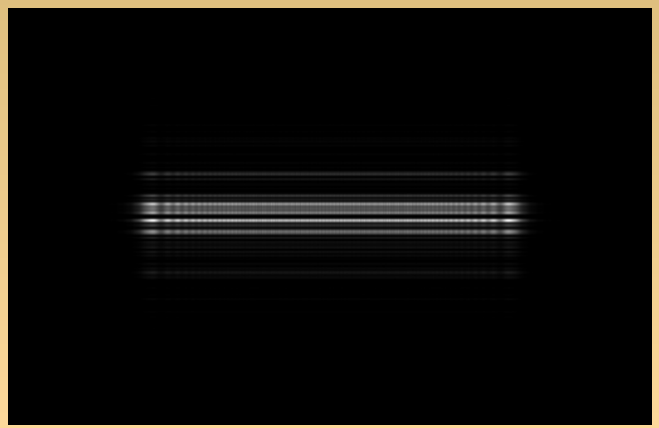

6.2 keV

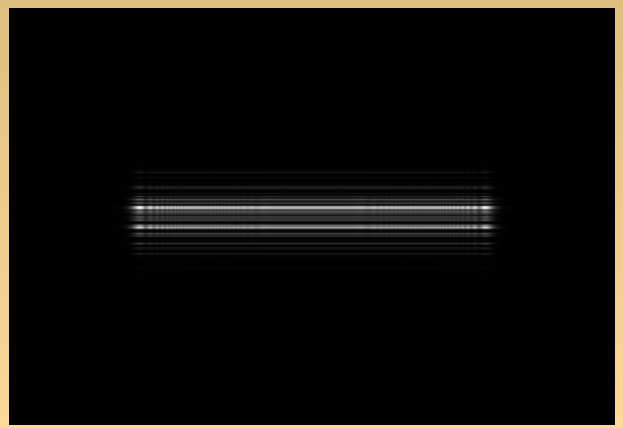

12.4 keV

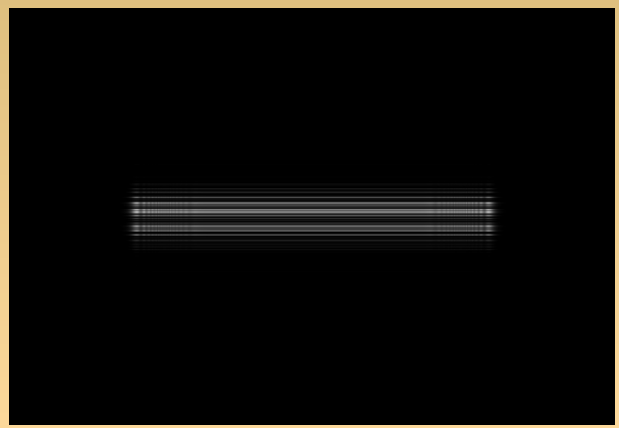

24.8 keV

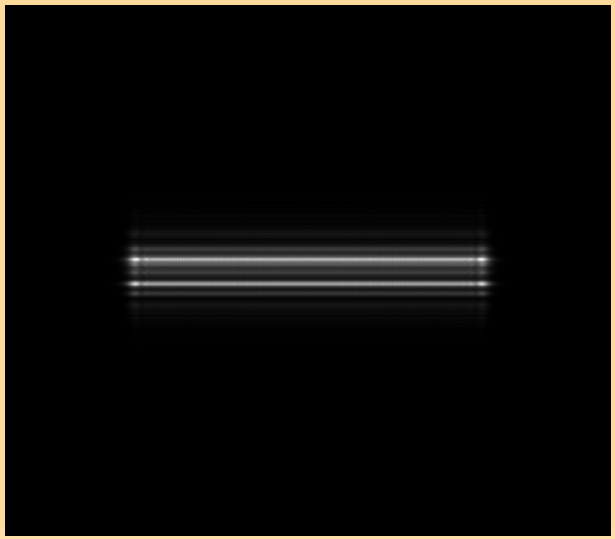

Averaged over spectrum

Use iterative reconstruction techniques

URA 1x31 x 4 um; Iterative reconstruct.; Beam sigy=5 um, 5-30 keV; 10% Noise

Source Image

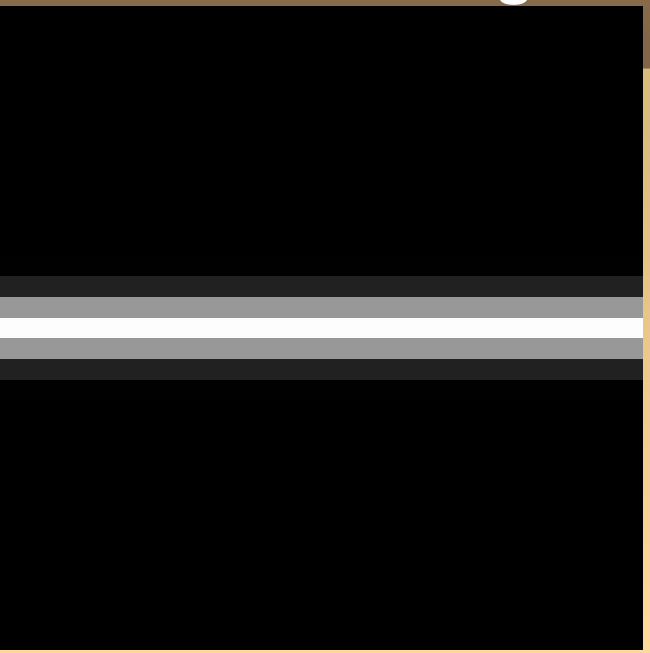

Mask Irradiance w/diffraction

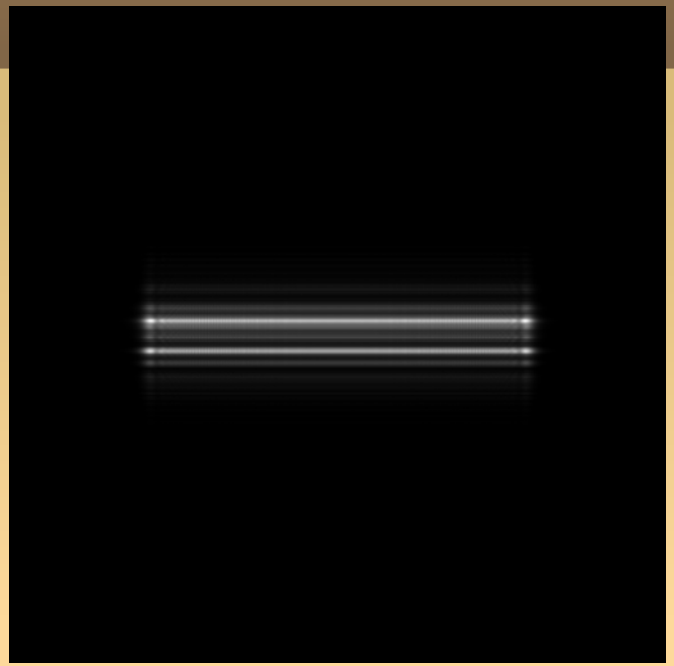

Detector Image

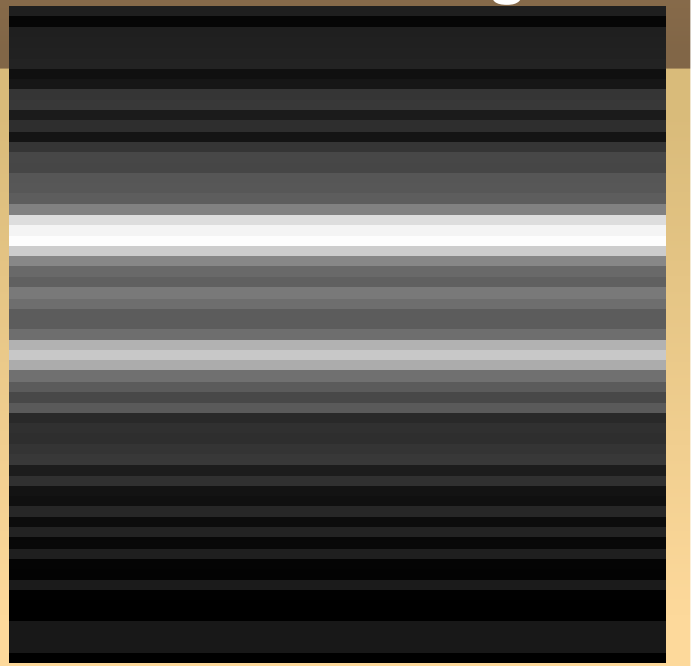

Reconstructed Image and Profile

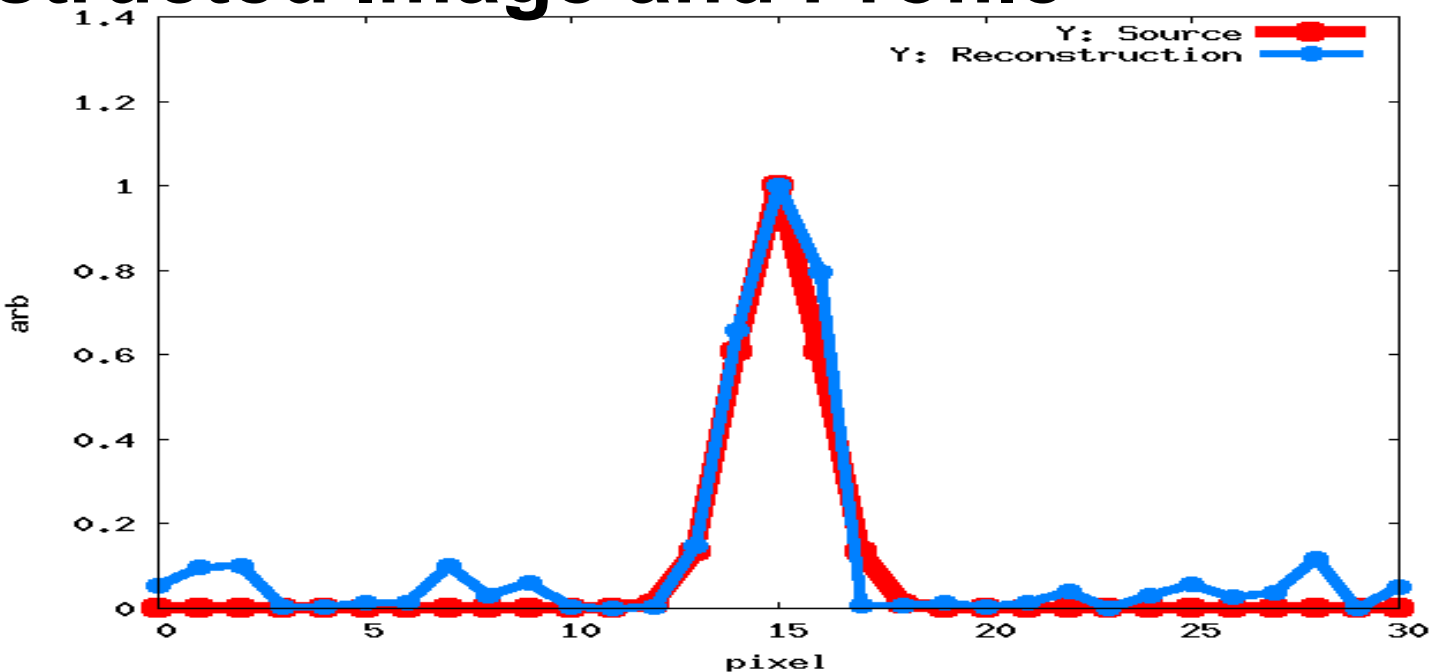

Index of refraction also cannot be ignored

$$n = (1 - \delta) + i\beta$$

Phase shift

Attenuation

- At high energies the transmission and phase shift through mask region becomes significant.

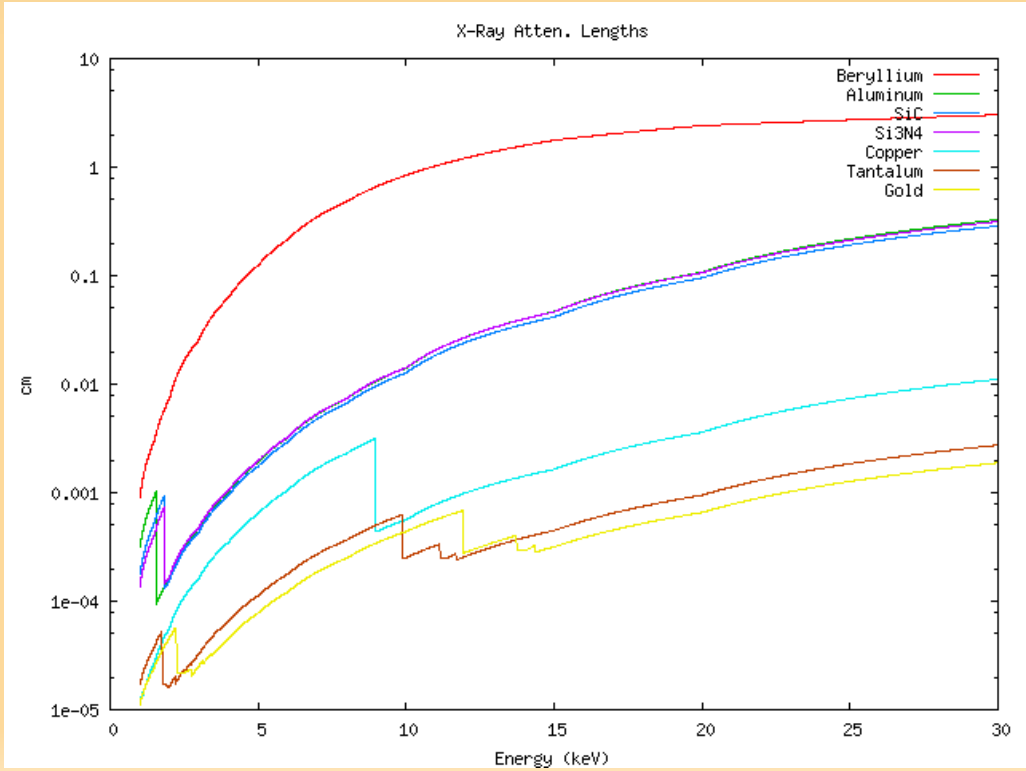

Simulation Including Transmission/Refraction

Mask: 

Example @ 0.1 A (1.2 keV)

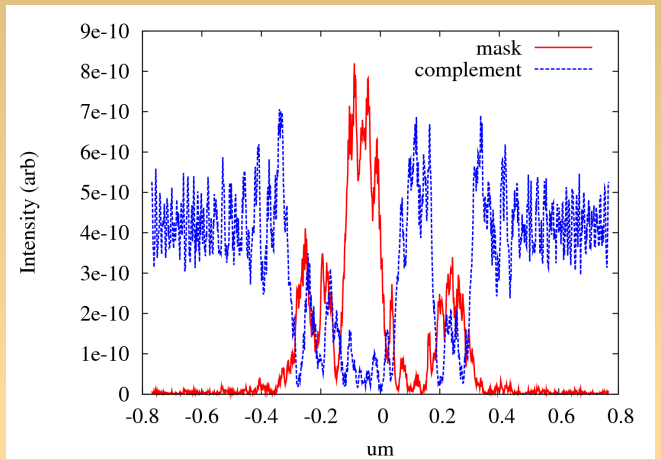

Mask & Complement Intensity

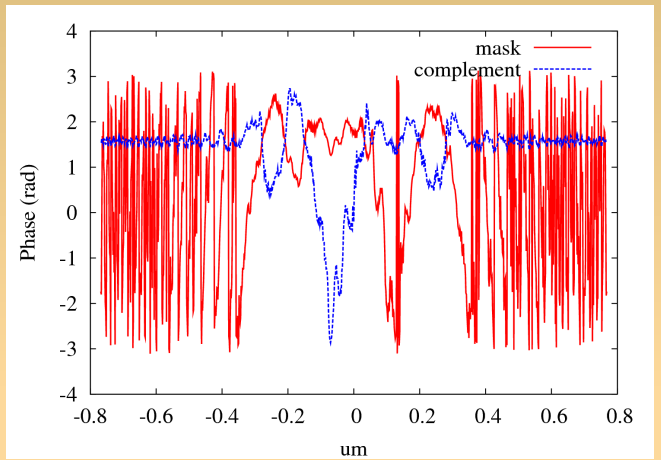

Mask & Complement Phase

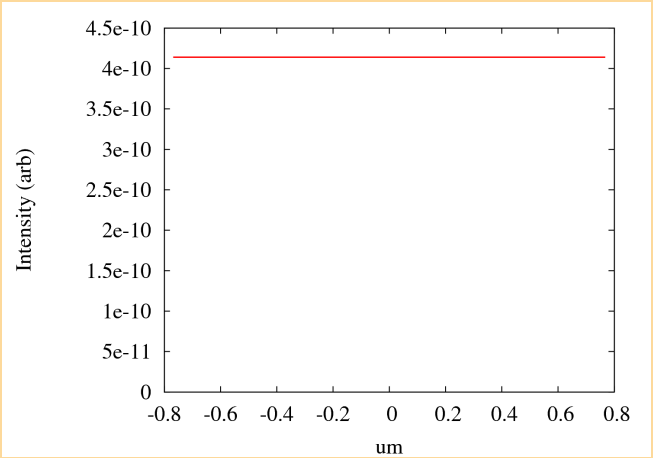

Simple Vector Sum Intensity (Babinet check)

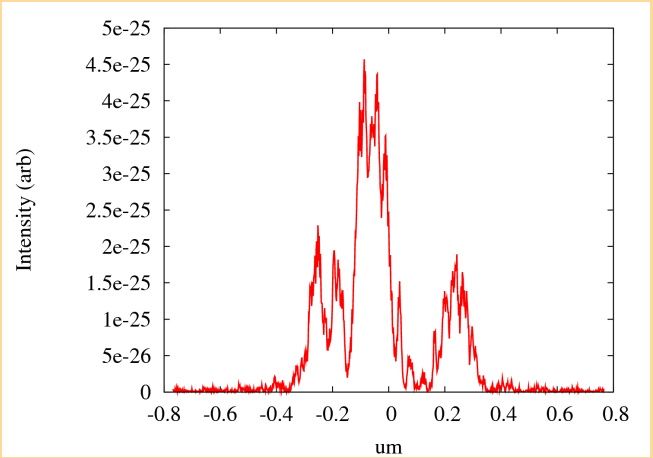

4 um Ta Mask Intensity

- At each wavelength, calculate effective mask pattern from phase and amplitude data of mask and complementary mask, apply attenuation and phase shift from mask material, then add vectorially
  - Zemax (commercial program) used for wavefront calculations.
- Do weighted sum over relevant wavelength range to get **effective mask pattern**.

Simulation verification

- Test slit pattern fabricated
- Varying slit widths from 5-40 um
- Will test with narrow-band x-ray beam to verify simulated response function in detail.

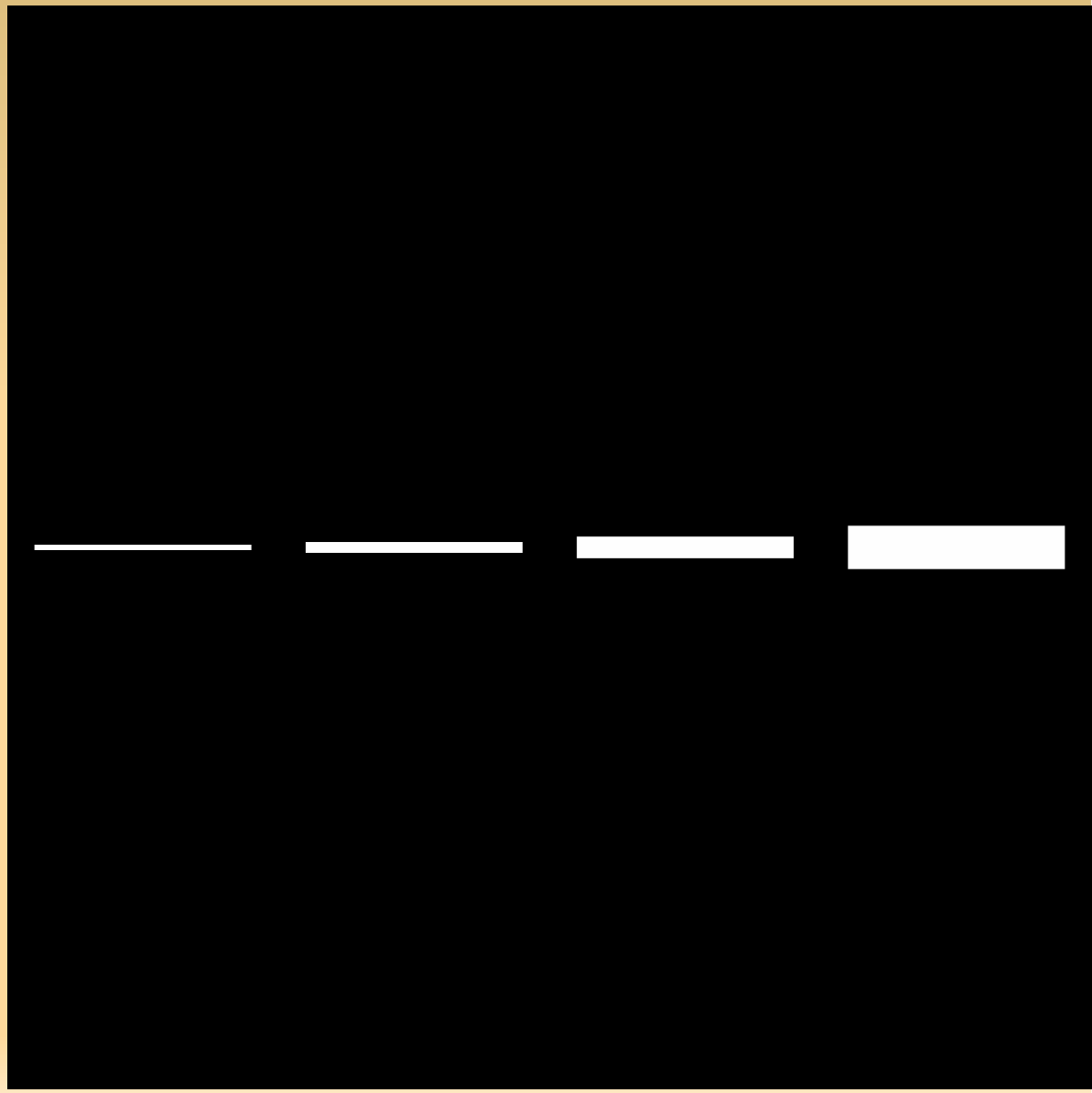

Prototype Tests at CESR-TA

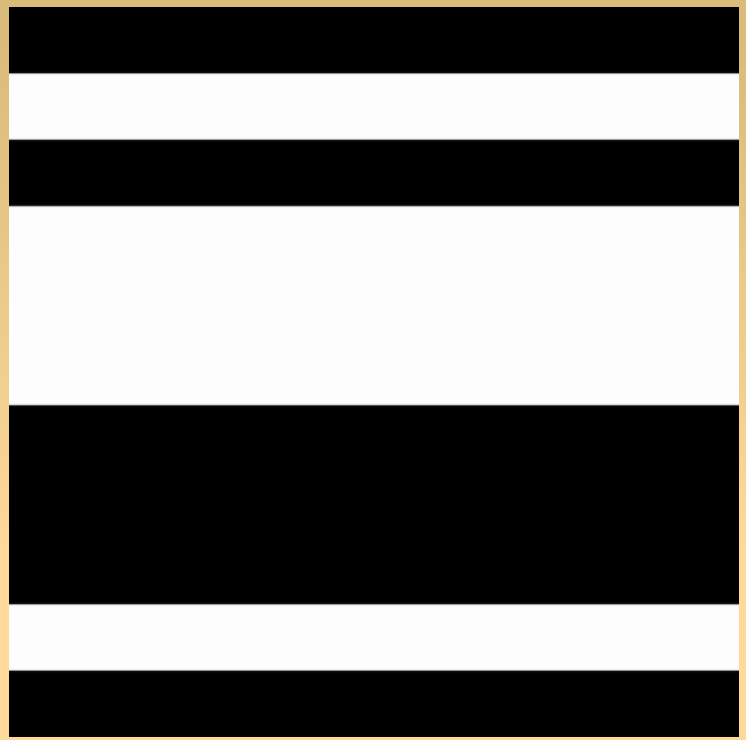

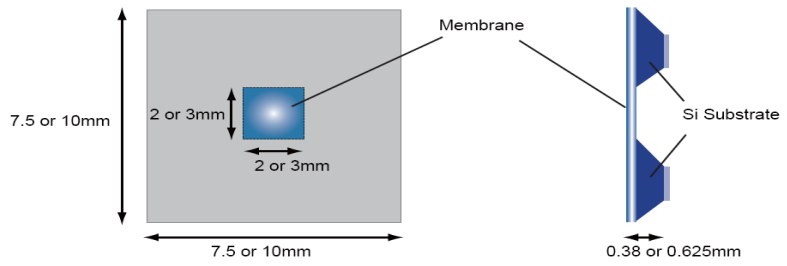

Schematic of Membrane

Renarks:
The specifications stated in this brochure are representative values
and not guaranteed. Also, please kindly note that the specifications may change without prior notice for product update.

NTT Advanced Technology Corporation
International Sales and Marketing Department
Musashino Center Building 6F, 1-19-18, Naka-cho,
Musashino-shi, Tokyo, 180-0011, Japan
TEL : +81 422 36 6715
FAX : +81 422 36 6702
E-mail : moreinfo@ntt-at.co.jp
URL : http://www.ntt-at.com

- Started testing of prototype mask at CESR-TA
  - 4 um Ta mask made by NTT-AT
- Using CHESS user beamlines, can observe 2.1-5.3 GeV beams.
- Vertical beam sizes from 30-150 um, eventually down to ~10 um at low energy.

June 2008 Beamline Layout

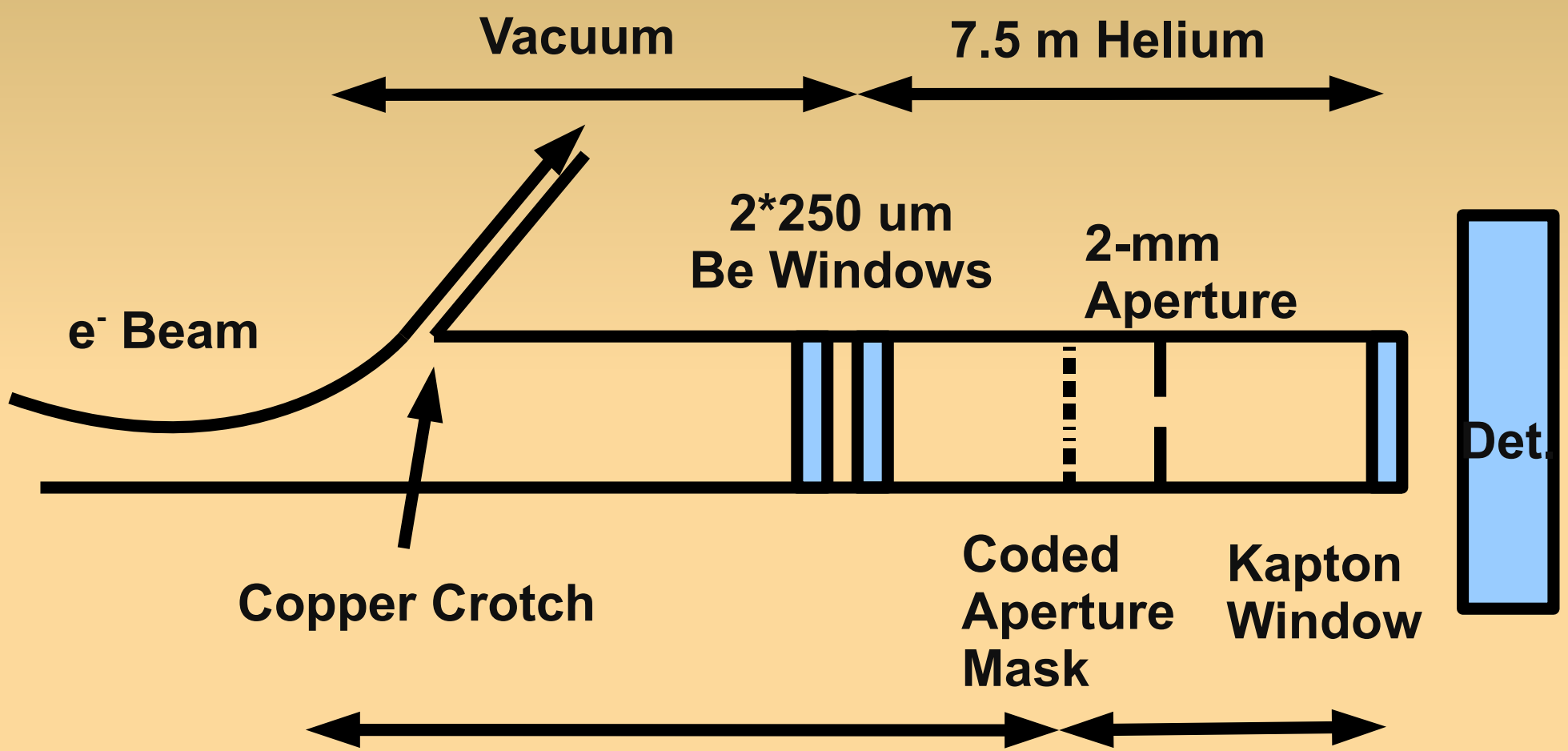

CHESS B Line

Mount for Coded Aperture Mask and Slits

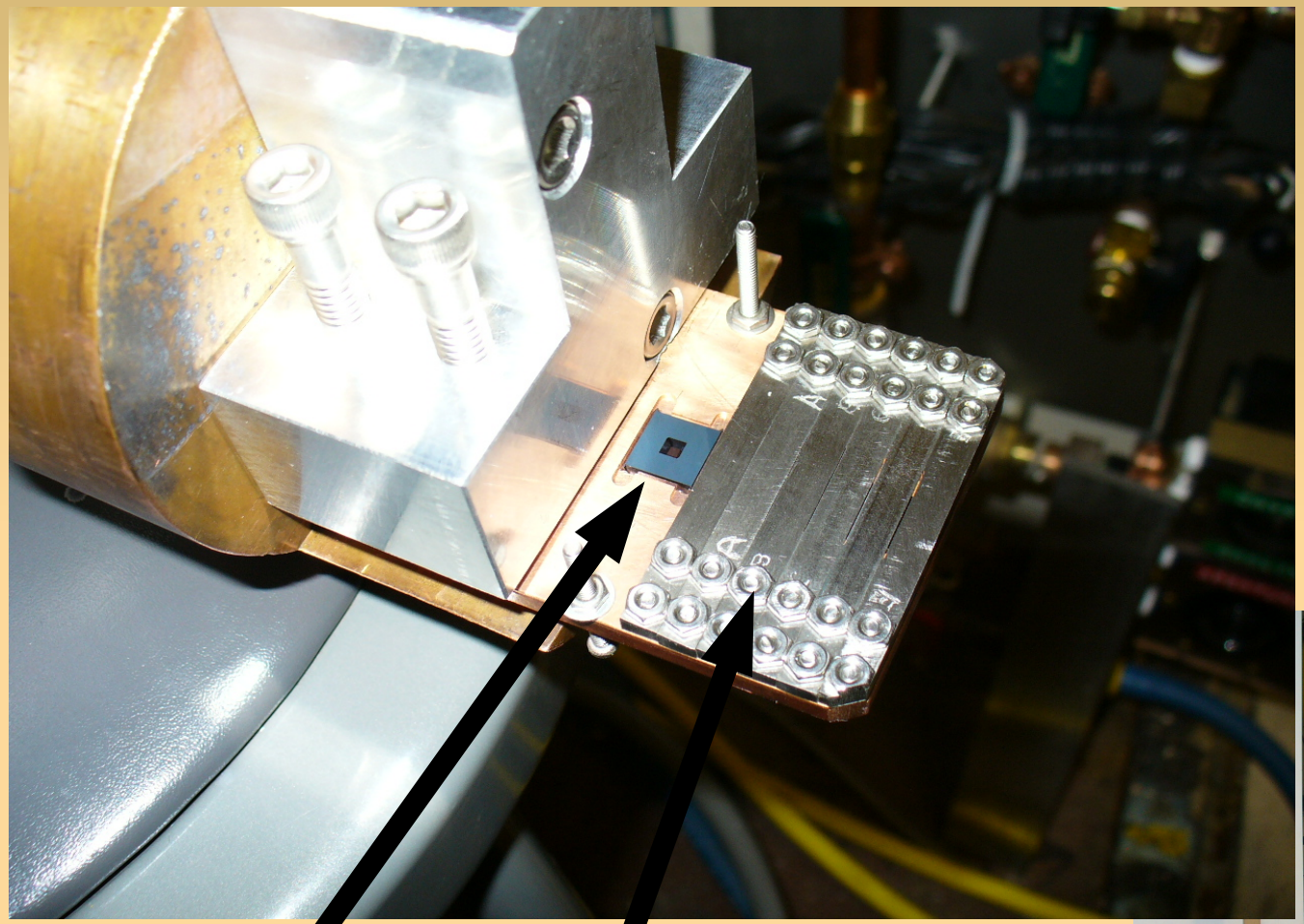

Mount
location
in beamline

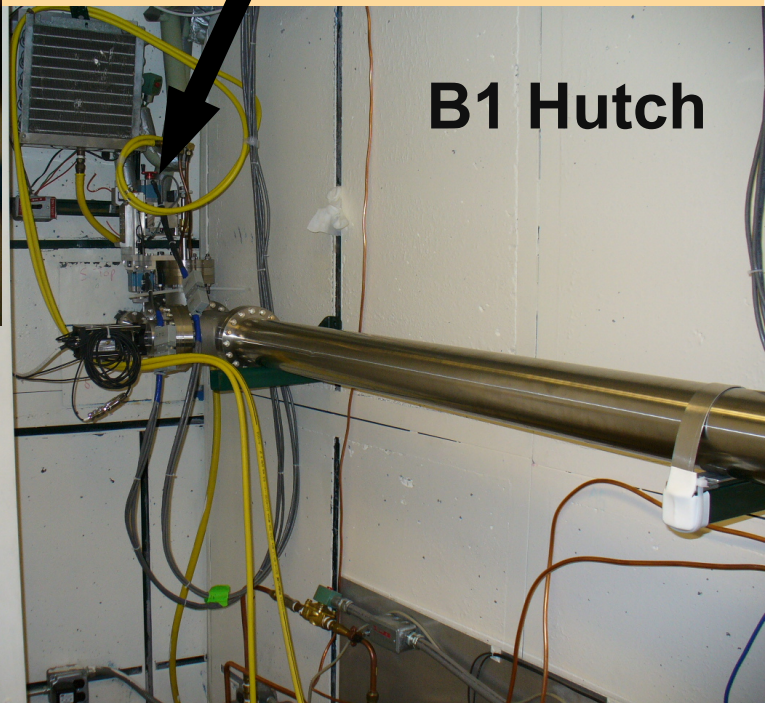

CA Mask

Slits (40-200 um)

Heat Load

- Calculated heat load due to X-radiation absorbed in tantalum not a problem at 2.1 GeV.
- At 5.3 GeV, Al filter needed to cut down heat load to manageable levels.
  - Si backplane in mask region would help at high-energy, but would be too absorbing at 2.1 GeV.

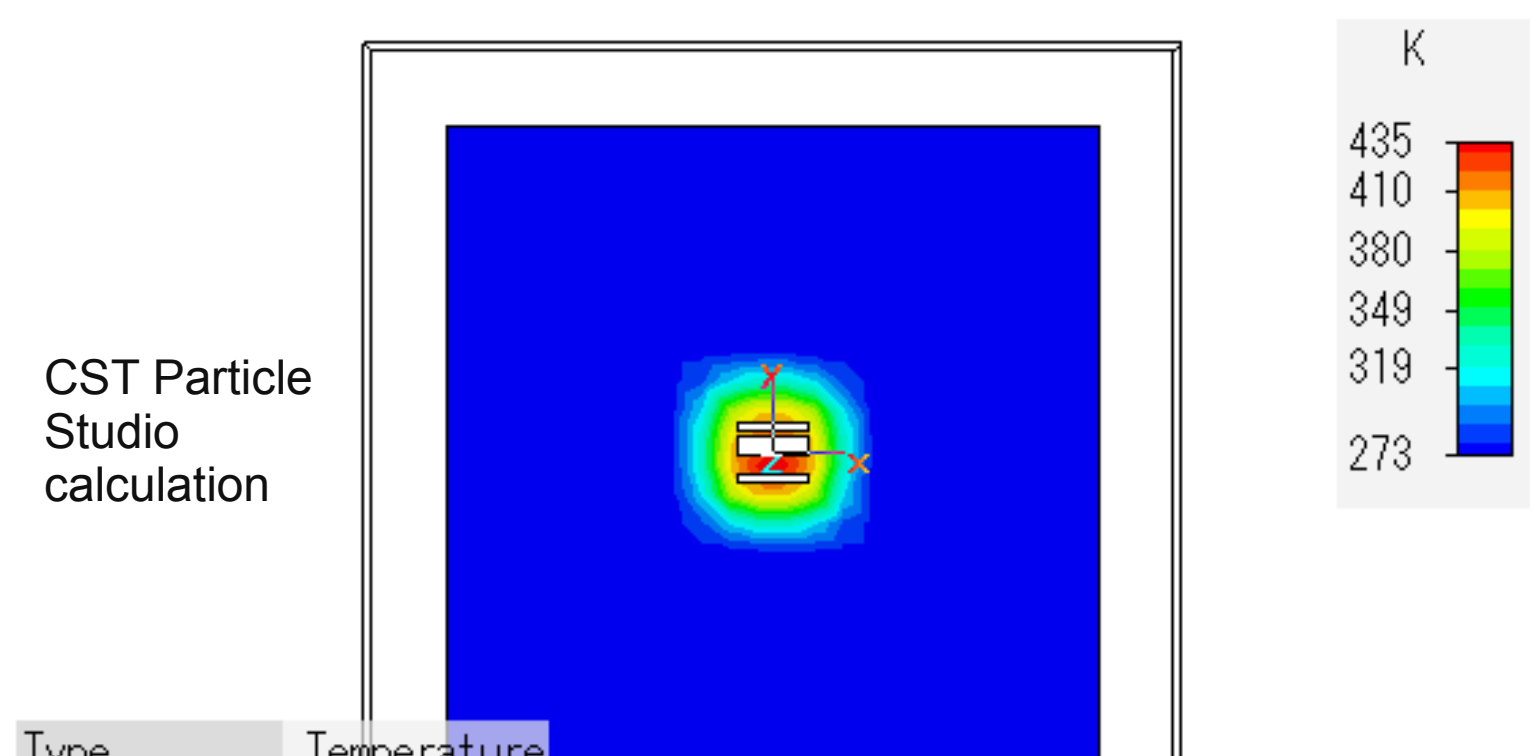

Prototype testing at CESR-TA

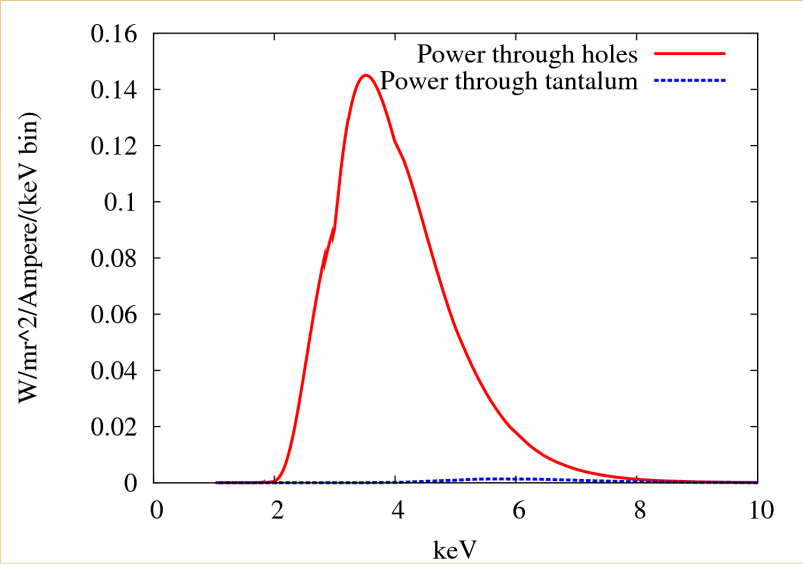

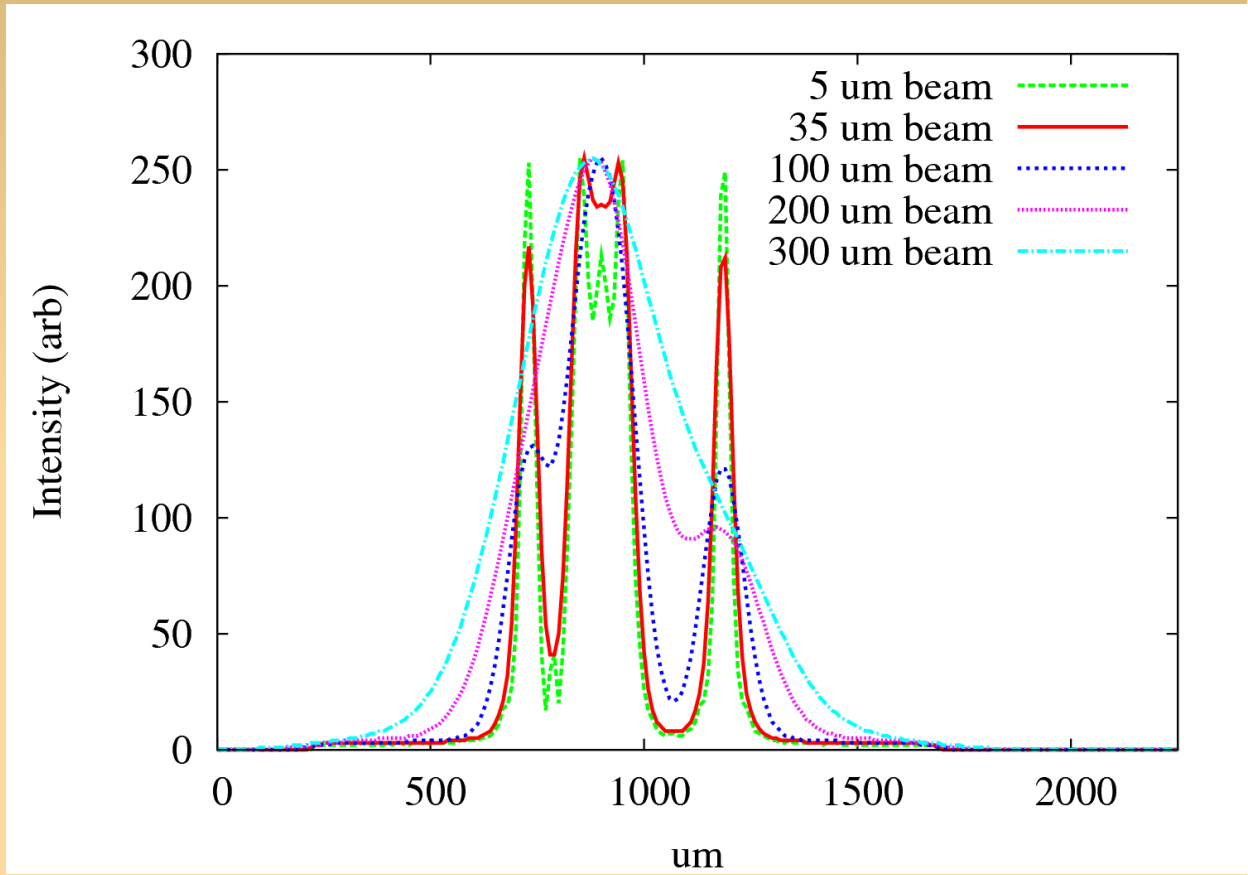

- X-ray spectrum, and simulated detection pattern for CESR-TA at **2.1 GeV**.

Prototype testing at CESR-TA

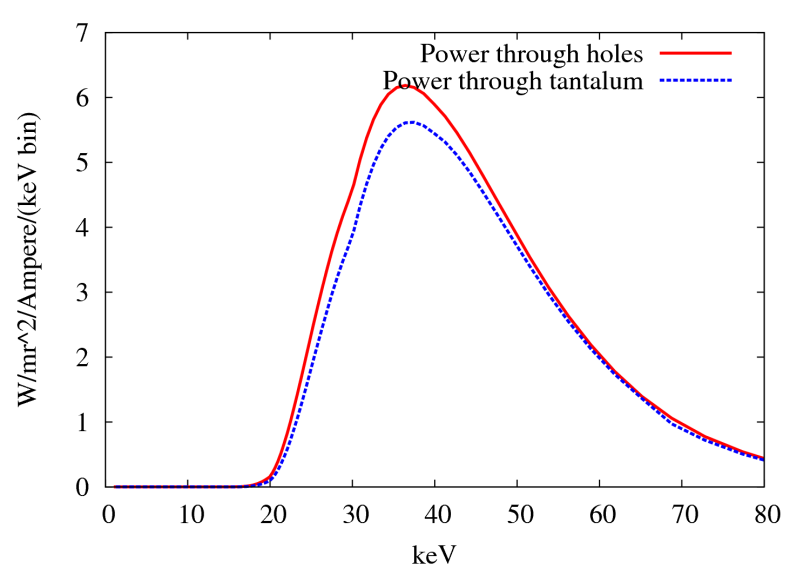

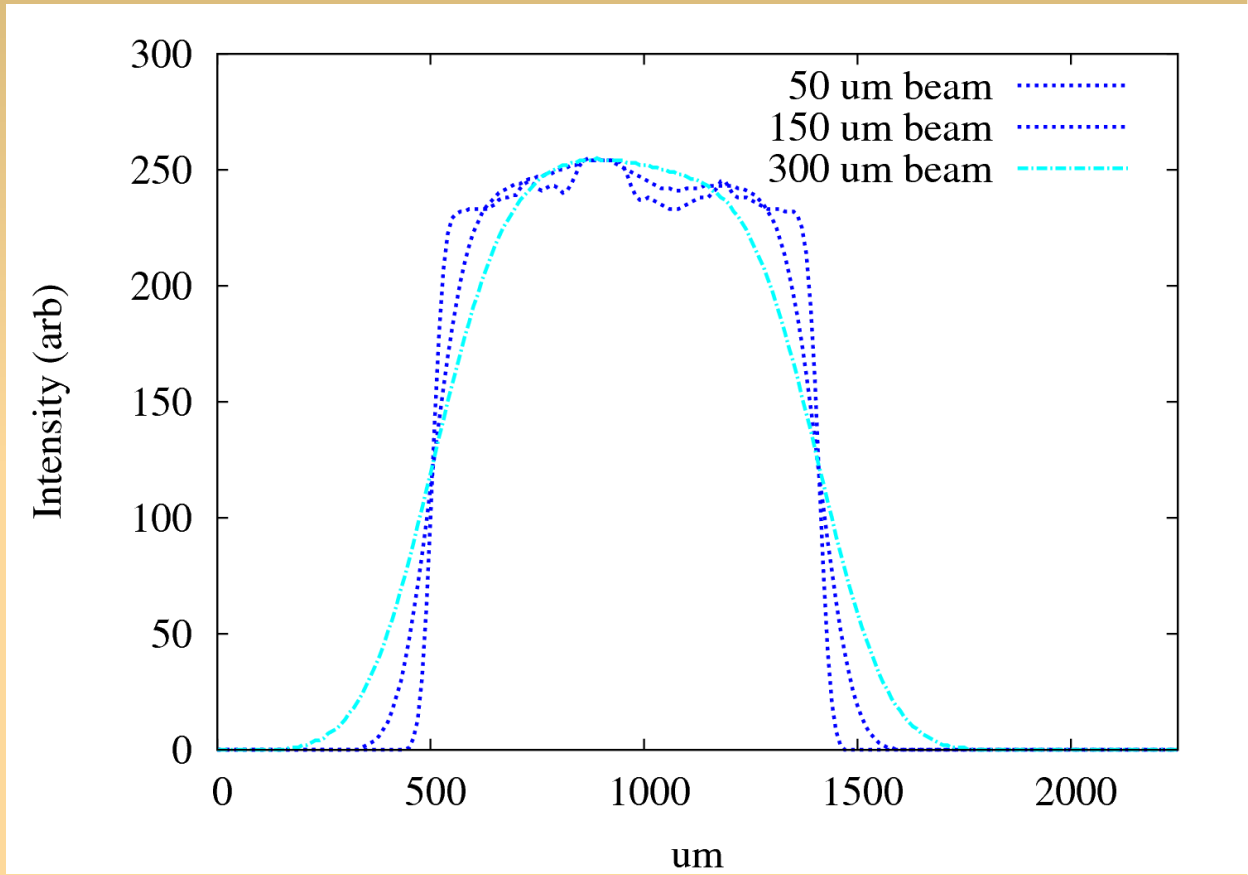

- Xray spectrum, and simulated detection pattern for CESR-TA at **5.3 GeV**.

Coded Aperture: "Thin" beam
Very Preliminary!

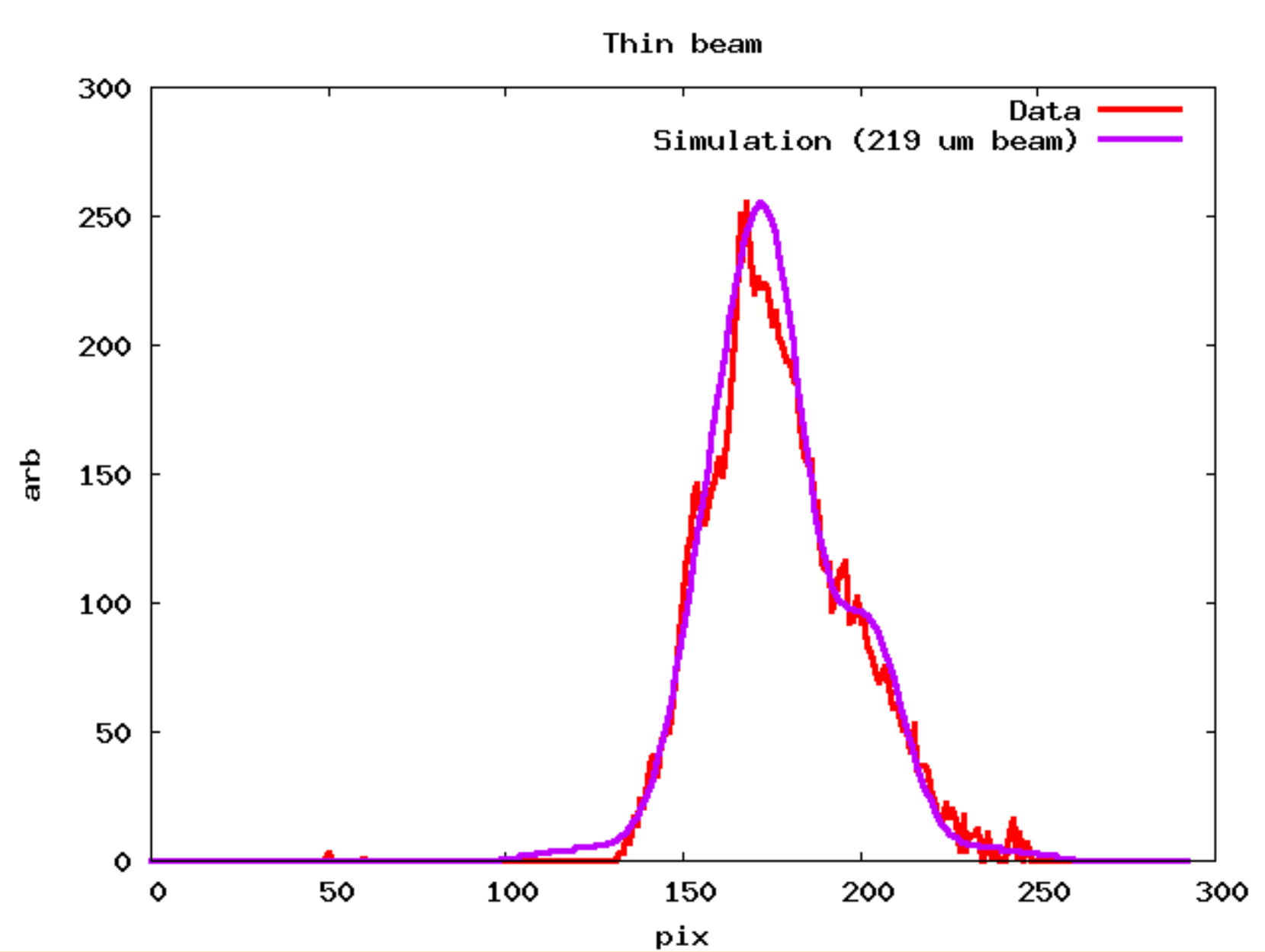

Coded Aperture: "Fat" beam
Very Preliminary!

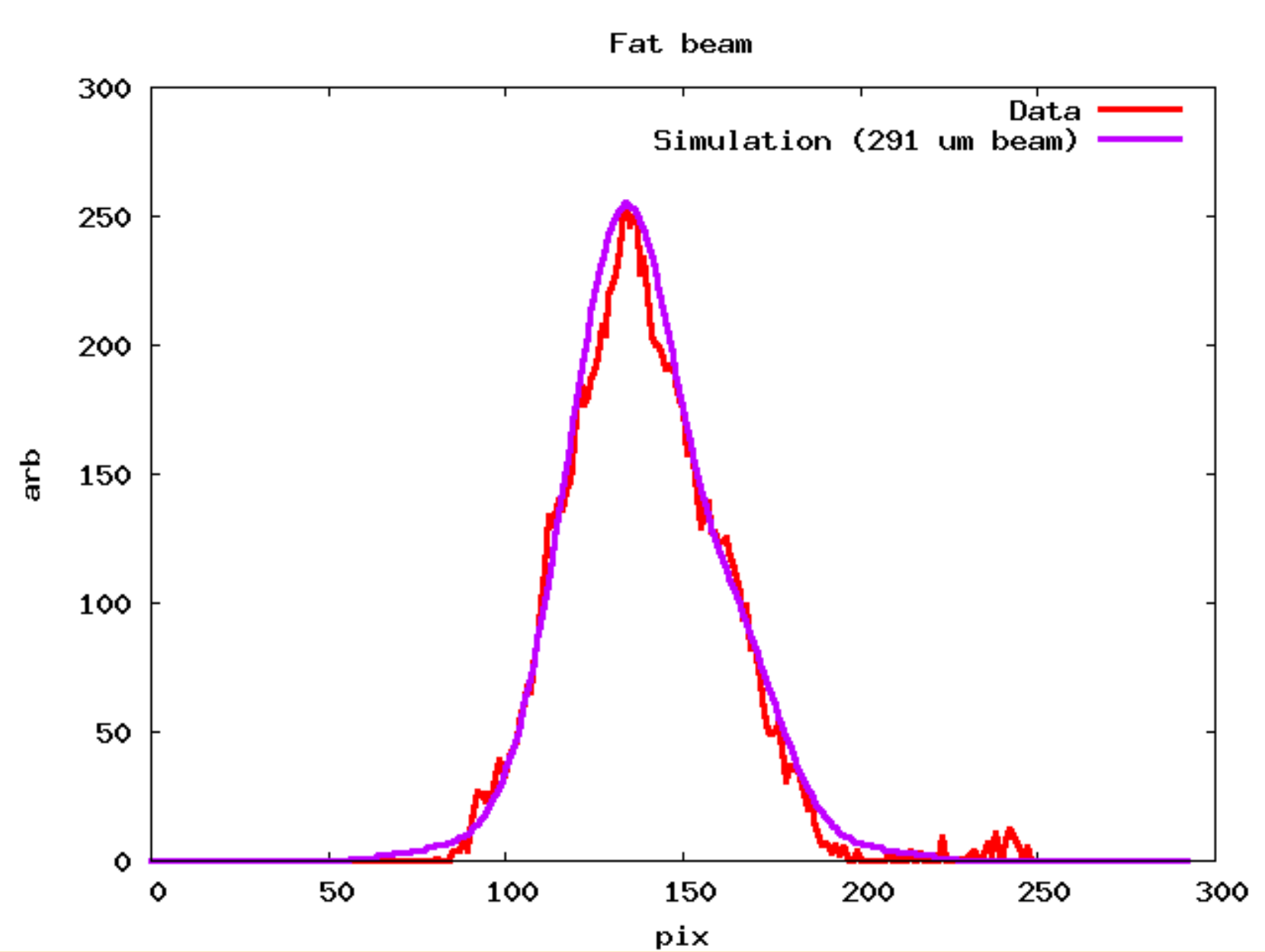

40 um Slit: “Thin” beam
Very Preliminary!

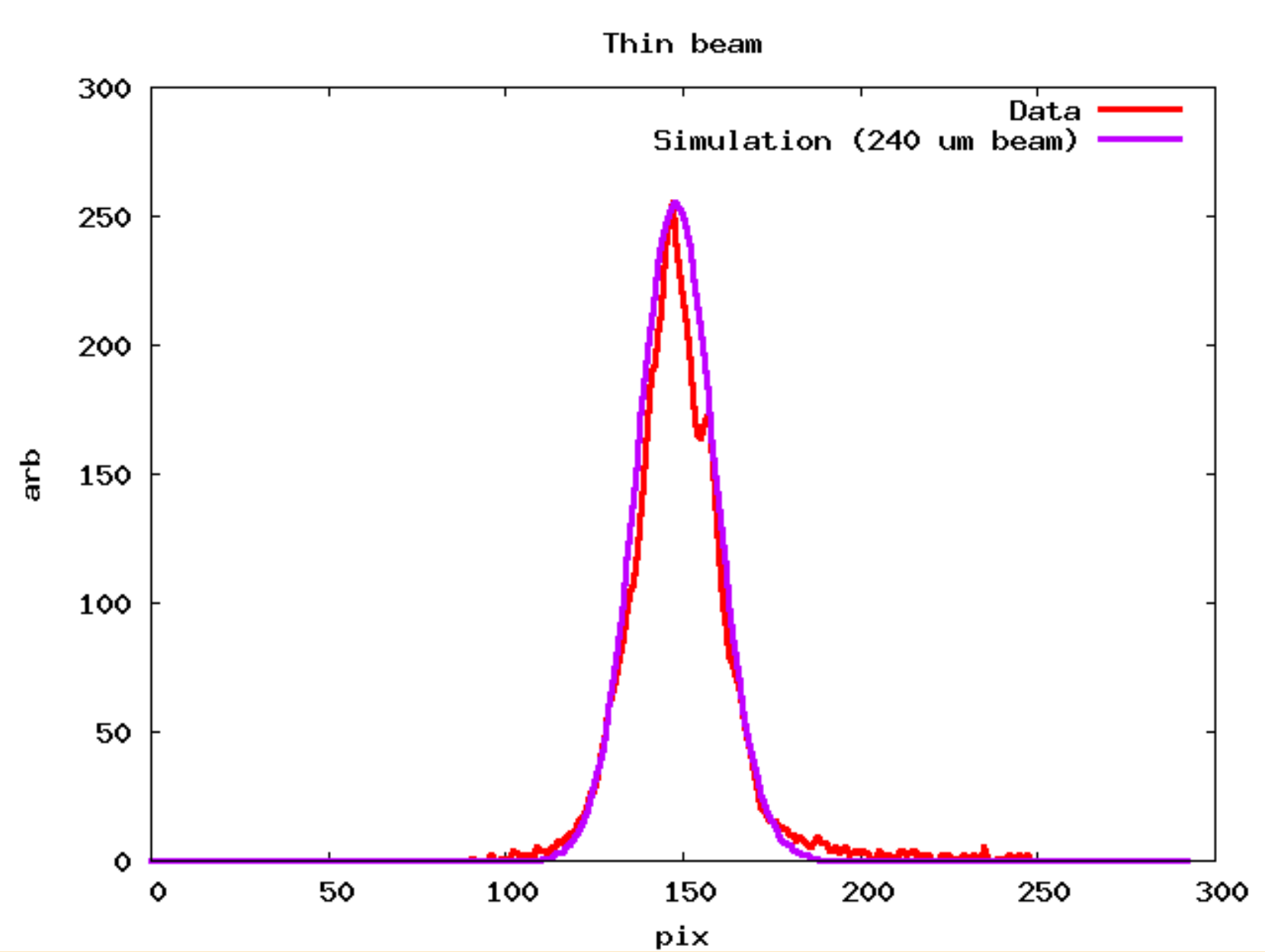

40 um Slit: "Fat" beam
Very Preliminary!

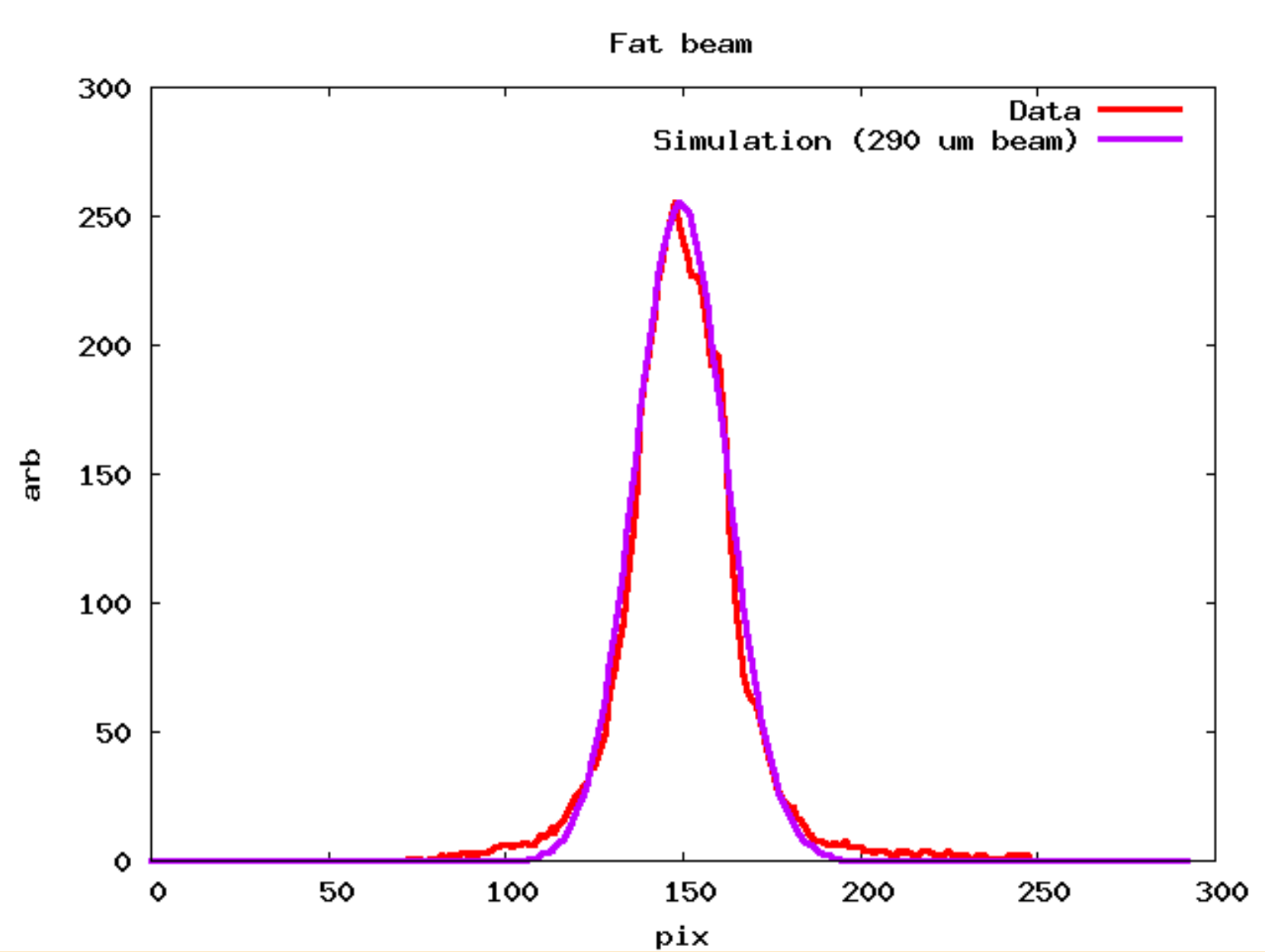

Why does the beam look so fat?

- 1) Scattering?
  - Bulk scattering: of all components in beamline, largest scattering cross-section is for Helium
    - Compton scattering angular distribution (Klein-Nishina):
    - $$\frac{d\sigma}{d\Omega} = \frac{1}{2} r_e^2 \left(\frac{E_{out}}{E_{init}}\right)^2 \left[\frac{E_{init}}{E_{out}} + \frac{E_{out}}{E_{init}} - \sin^2\theta\right]$$
    - Too broad: distribution looks like 1+cos^2 (elastic case) or broader when averaged over full outgoing spectrum
    - =>Must contribute to diffuse background rather than to beam image smearing
  - Note: low-energy helium Compton scattering cross section is apparently not well-described by standard theory (Kraessig et al., Intl. Workshop on Atomic and Molecular Physics at High Brilliance SR Facilities, Hyogo, Japan (1998)) (Ref. from G. Varner)
    - Need more study?

Energy dependence of attenuation and scattering

(Ref.: NIST website, http://physics.nist.gov/PhysRefData/XrayMassCoef/tab3.html)

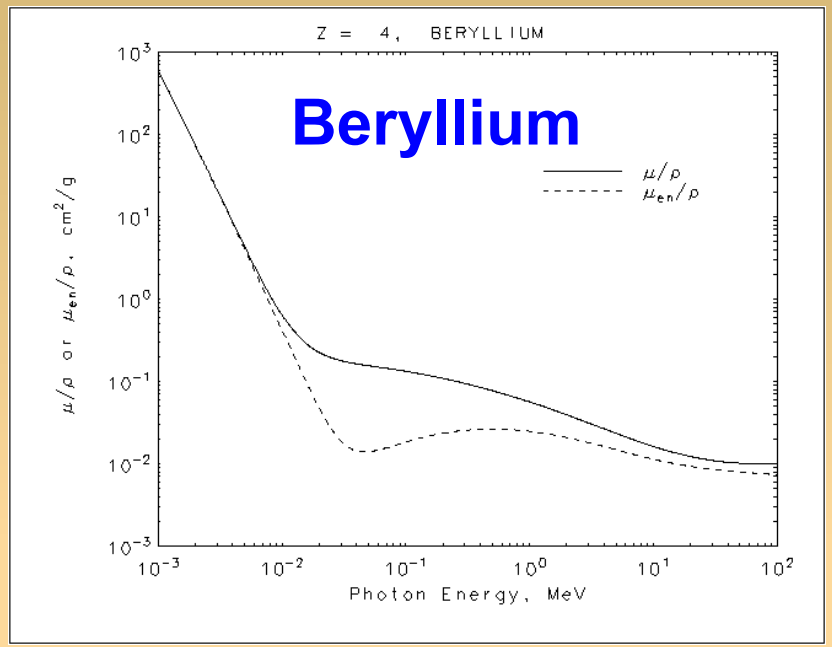

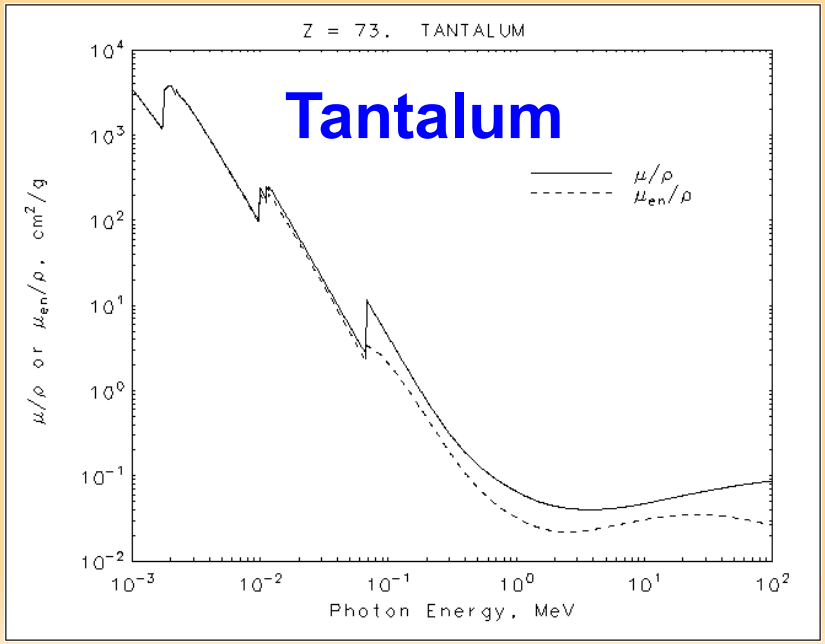

Absorption

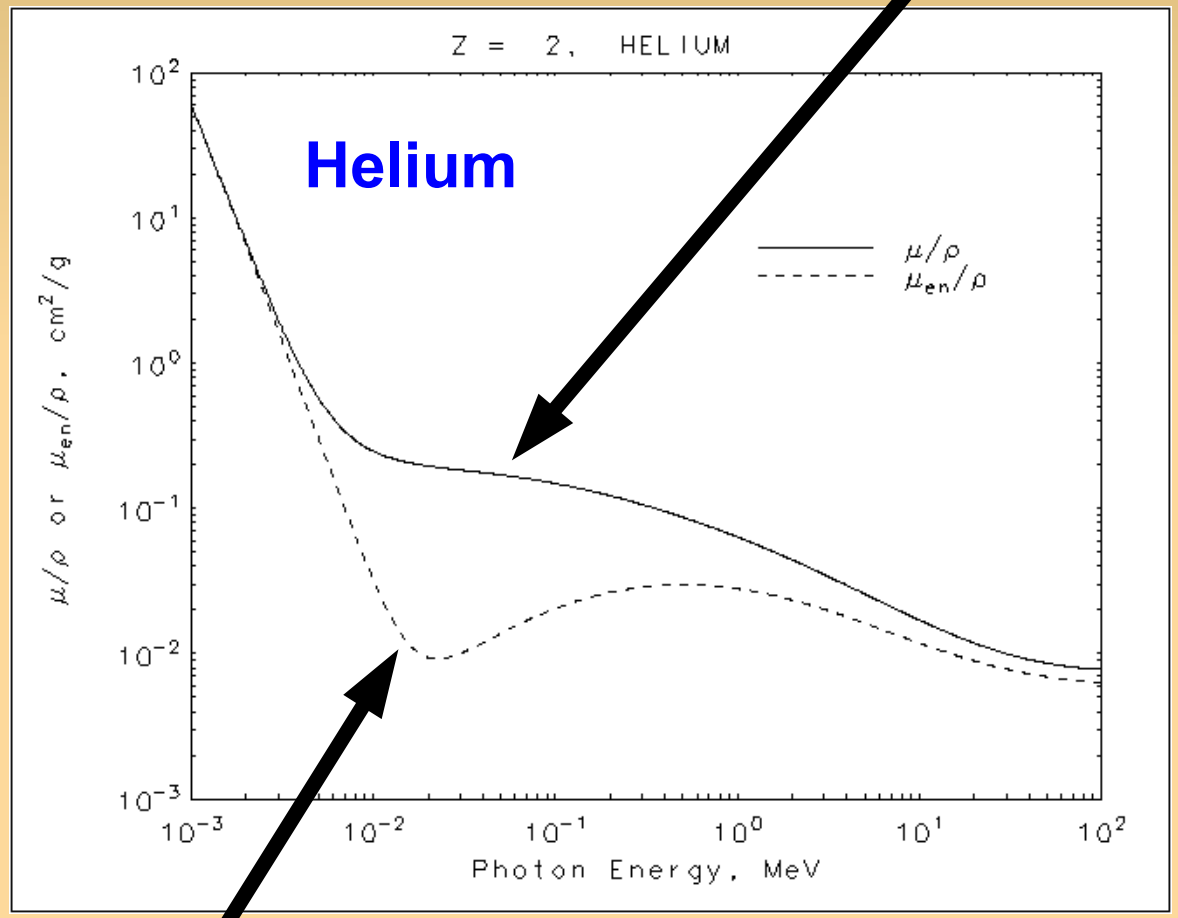

Scattering (Compton, Rayleigh)

Why does the beam look so fat?

- 1) Scattering? (cont.)
  - Surface scattering (grazing incidence) candidate locations:
    - Upstream copper crotch
    - Downstream 2 mm-wide aperture
    - Something else?
      - Take a look this week
- 2) Tilt?
  - Either beam or beamline tilted?
- 3) Pixel cross-talk/bleed-through?
  - Even treating the nominally 25 um-high pixels as 100 um high does not reproduce results.

Background

- Background profile is noticeably non-flat.
- Ridges in beryllium surface?
- Fat beam structure looks a bit more smeared than thin beam shape. (Think of Be striations as coded aperture.)
- Calculated feature size would be ~25 um if Be
  - 5.3 GeV data suggest somewhat smaller feature size.
- If iron accretions, then ~1 um
  - Iron accretions reportedly observed by CHESS folks.

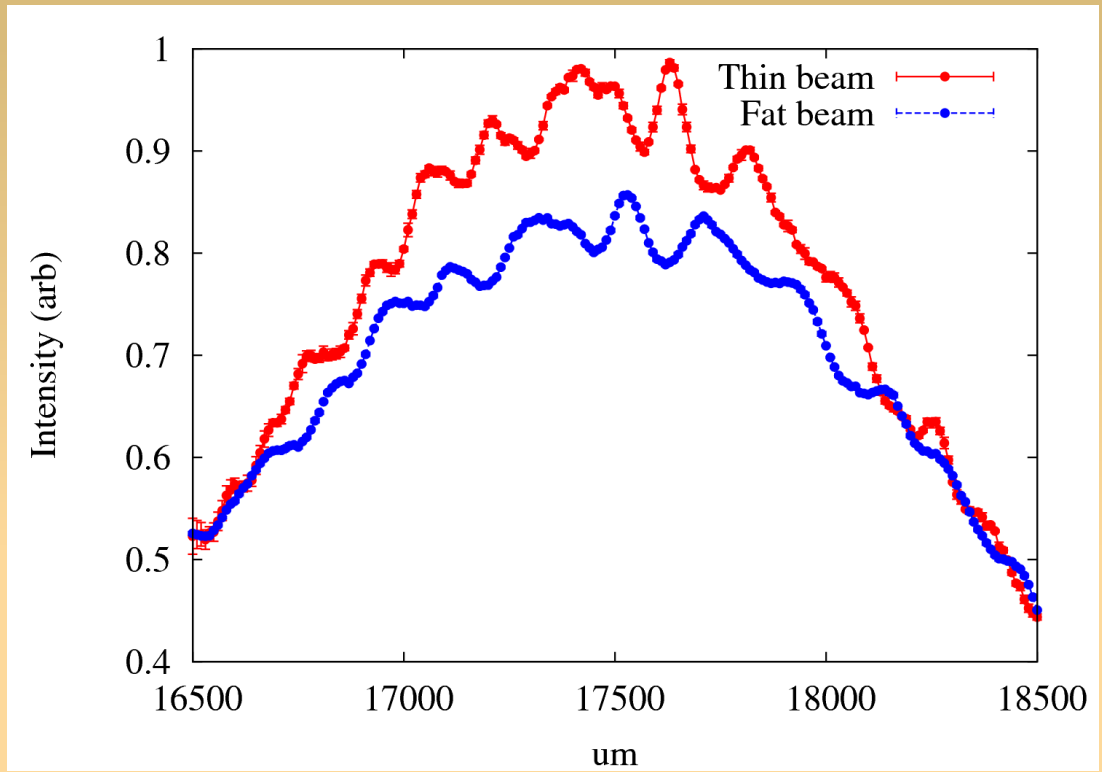

- **Beam sizes may look smaller if this is properly modelled**
  - Treat as second coded aperture upstream of mask/slit?
  - **However, even with that the modulation depth is too small to turn a 35 um beam into a >200 um one.**

Could the beam really have been fat?

- According to Mike Billing, “quite possible.”
  - Large angle bump needed to get beam down the CHESS B line, may have leaked around the ring
    - Previous day's orbit looked already to have large (3 mm) vertical COD modulation around ring.
  - He has graciously offered to go spelunking through records to see if beam condition can be reconstructed.
    - **==>DONE! Estimated beam size was 203 um.**
- Image monitor may provide supporting evidence.
  - Image noticeably changed when beam was blown up.
  - PSF of ~150 um suggests that we should not have been able to see a change from 35 um -> 70 um.

Summary

- Measurements made at 2.1 GeV at CHESS B line show beam show difference between “thin” and “fat” beams.
- However, beams looks much larger than expected, with both Coded Aperture and 40 um slit:
  - “Thin” beam ~220-240 um? (expected ~35 um?)
  - “Fat” beam ~290 um? (expected ~70 um?)
    - Proper reconstruction requires more careful understanding & treatment of background, “beryllium striations.”
- Cause not understood.
  - Examine beamline again this week.
  - Beam may really have been fat. (Mike Billing)
    - Estimated beam size 203 um (per Mike)
- Tentative plan
  - Use current mask again in Fall run – All-vacuum beamline, no upstream window, so fewer complications
  - Prepare finer mask for use in January or later

Extras

Gated Camera Observations of Trailing Witness Bunch

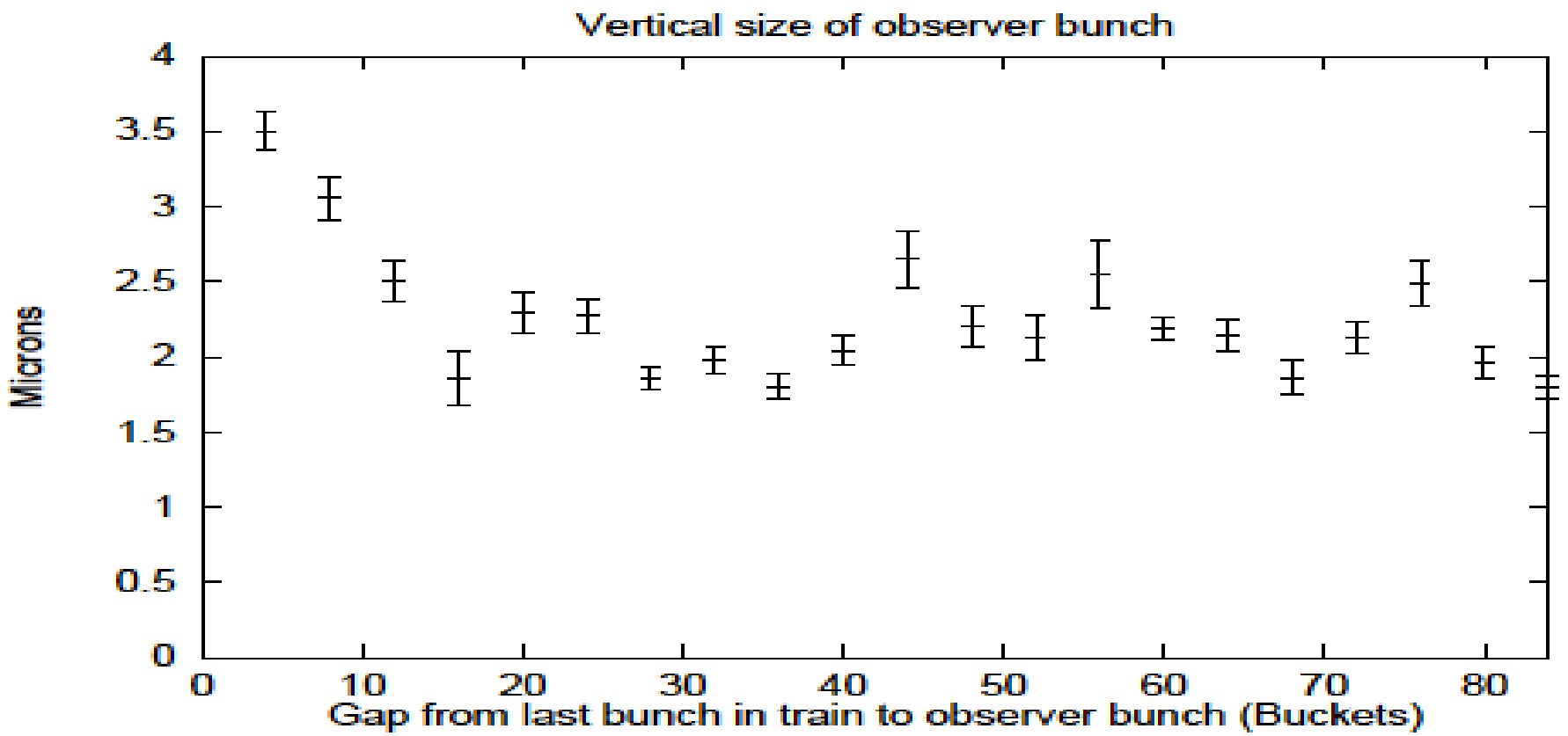

Figure 5: Dependence of size of trailing observer bunch size on distance to leading train.

J.W. Flanagan et al., Proc. EPAC00 (2000) 1119

Time Development of Instability: 512-turn slices

BPM data

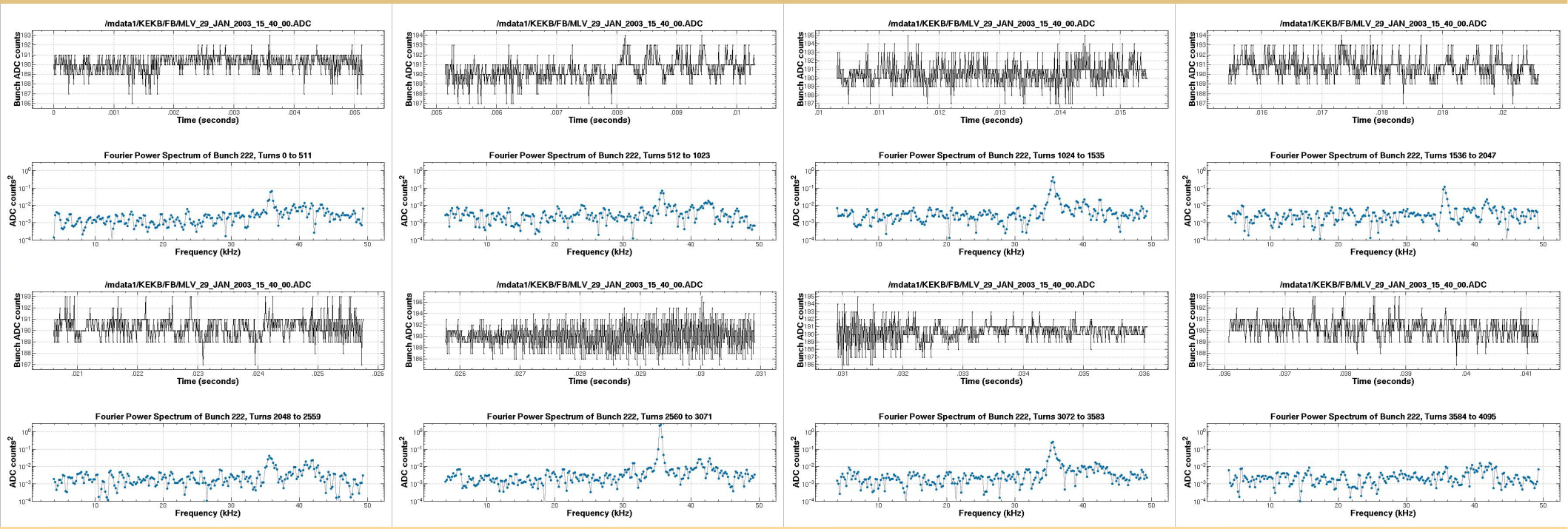

$$\rho_{e,th} = \frac{2\gamma\nu_s(\omega_e + \omega_0\xi_y/\alpha)\sigma_z/c}{\sqrt{3}KQr_e\beta L}, \quad (1)$$

This lack of threshold dependence on initial beam size can be explained by examining the beam size dependence in Equation 1, which comes in from ω_e:

$$\omega_e = \sqrt{\frac{\lambda_+ r_e c^2}{\sigma_y(\sigma_x + \sigma_y)}}, \quad (2)$$

where λ_+ is the beam line density in the bunch, r_e is the classical electron radius, and σ_x and σ_y are the horizontal and vertical beam sizes, respectively. As discussed in Reference [8], Q is a measure of the range of the effective wake due to the electron cloud, but since it can only act on the bunch within the length of the bunch, the effective Q is the lesser of either the natural Q or $\omega_e\sigma_z/c$. For KEKB, with a bunch length of ~ 5.5 mm, $\omega_e\sigma_z/c \approx 5$, which is at the lower end of a numerical estimate for Q of $5 - 10$ for a coasting beam[9]. Substituting $\omega_e\sigma_z/c$ for Q in Equation 1, and noting that $\omega_e \gg \omega_0\xi_y/\alpha$ for low values of ξ_y, the head-tail instability threshold is seen to be almost insensitive to the initial beam size σ_y. This agrees with the data; finer-grained data at higher chromaticity may show a measurable change in threshold.

Motivation (cont.)

- KEKB currently uses:
  - SR Interferometers
    - High resolution, but narrow band: no single-bunch measurements
  - Streak cameras, gated cameras:
    - Wideband with reflective optics, but low resolution
- Both systems used at KEKB are also sensitive to mirror distortion due to SR heat load, which introduces beam current dependence to beam size measurements..
- Decided to look into use x-ray monitor.